Bio-Design and Manufacturing (2026) 9:206–239
https://doi.org/10.1631/bdm.2500639

REVIEW

Shaping the future of biofabrication and biomanufacturing in Singapore

Wei Long Ng[1] · Marin Zhen Lin Yee[2] · Kee Woei Ng[2,3,4] · Yanjiao Teng[5,6] · Seeram Ramakrishna[5,6] · Yanting Liu[5] · Swee Leong Sing[5] · Sharon Mui Ling Nai[7] · Kun Liang[4,8,9] · Hong Liang Tey[4,8,10] · Adrian Kee Keong Teo[11,12,13,14] · Andri K. Riau[15,16] · Jodhbir S. Mehta[15,16,17] · Jia Min Lee[1] · Xi Huang[1] · Wai Yee Yeong[1,18] · Boyang Huang[1] · Cian Vyas[1] · Paulo Bartolo[1]

Received: 15 December 2025 / Accepted: 21 January 2026

Abstract

Biofabrication and biomanufacturing are rapidly transforming how materials, therapeutics, and functional biological constructs are produced. These fields integrate developments in sustainable biomaterials, precision fabrication, biological systems, and data-driven engineering to produce scalable, efficient, and environmentally aligned production pathways. This review highlights recent scientific advances led by researchers in Singapore, focusing on three interconnected pillars: sustainable bio-derived materials, enabling fabrication and manufacturing technologies, and emerging applications. We first examine the expanding use of biomass-derived feedstocks, including human hair keratin, aquaculture side-streams, and plant-derived polysaccharides, which support circular and resource-conscious material development. We then present advances in biofabrication technologies, including electrospinning, three-dimensional bioprinting, and metal additive manufacturing, that enable improved control over the structure, function, and manufacturability of biomedical and functional constructs. Emerging applications, such as machine learning-assisted additive manufacturing, food biomanufacturing, regenerative cell therapy, microneedles, and bioelectronics, exemplify how biofabrication and biomanufacturing are increasingly interrelated across the health, materials, and technological domains. These research contributions from Singapore exemplify how sustainable feedstocks, digital and automated fabrication platforms, and biologically driven applications are shaping the evolving landscape of biofabrication and biomanufacturing. The convergence of materials science, biological engineering, and advanced manufacturing continues to enable new opportunities for innovation in biomedical, industrial, and societal contexts.

✉ Wei Long Ng
ng.wl@ntu.edu.sg

✉ Paulo Bartolo
pbartolo@ntu.edu.sg

1 Singapore Centre for 3D Printing, Nanyang Technological University, Singapore 639798, Singapore

2 School of Materials Science and Engineering, Nanyang Technological University, Singapore 639798, Singapore

3 Nanyang Environment and Water Research Institute, Nanyang Technological University, Singapore 637141, Singapore

4 Skin Research Institute of Singapore, Singapore 308232, Singapore

5 Department of Mechanical Engineering, College of Design and Engineering, National University of Singapore (NUS), Singapore 119077, Singapore

6 Department of Mechanical Engineering, Tsinghua University, Beijing 100084, China

7 Singapore Institute of Manufacturing Technology (SIMTech), Agency for Science, Technology and Research (A*STAR), Singapore 636732, Singapore

8 Lee Kong Chian School of Medicine, Nanyang Technological University, Singapore 308232, Singapore

9 A*STAR Skin Research Labs (A*SRL), Agency for Science, Technology and Research (A*STAR), Singapore 308232, Singapore

10 National Skin Centre, Singapore 308205, Singapore

11 Stem Cells and Diabetes Laboratory, Institute of Molecular and Cell Biology (IMCB), Agency for Science, Technology and Research (A*STAR), Singapore 138673, Singapore

12 Department of Biochemistry, Yong Loo Lin School of Medicine, National University of Singapore, Singapore 117596, Singapore

13 Department of Medicine, Yong Loo Lin School of Medicine, National University of Singapore, Singapore 119228, Singapore

14 Precision Medicine Translational Research Programme, Yong Loo Lin School of Medicine, National University of Singapore, Singapore 119228, Singapore

15 Regenerative Therapy Research Group, Singapore Eye Research Institute, Singapore 169856, Singapore

16 Ophthalmology & Visual Sciences Academic Clinical Programme, Duke-NUS Medical School, Singapore 169857, Singapore

17 Singapore National Eye Centre, Singapore 168751, Singapore

18 School of Mechanical and Aerospace Engineering, Nanyang Technological University, Singapore 639798, Singapore

Graphical abstract

Keywords 3D bioprinting · Biofabrication · Sustainable biomaterials · Food biomanufacturing · Cell therapy · Microneedles · Bioelectronics

1 Introduction

Biofabrication and biomanufacturing are closely related, rapidly evolving disciplines at the intersection of materials science, biotechnology, and biomedical engineering. Although the two terms are often used interchangeably, they represent distinct but increasingly interconnected domains. Biofabrication is the automated, spatially controlled assembly of biological and biofunctional constructs via additive manufacturing (AM), patterning technologies, and cell-instructive microenvironment engineering. Conversely, biomanufacturing has conventionally referred to the scalable production of biological products, including therapeutic molecules, biomaterials, food components, and engineered tissues, using cells, enzymes, and microbial systems. In modern practice, these conceptual boundaries are increasingly blurred, as living cells, advanced biomaterials, and digital manufacturing technologies are integrated to create functional biological products across the healthcare, food, and industrial sectors.

Driven by growing global demand for sustainable biomaterials, regenerative cell therapies, and next-generation therapeutic platforms, biomanufacturing has emerged as a central pillar of the emerging bioeconomy. This trajectory is evident in Singapore, where sustained long-term investments in biomaterials research, advanced manufacturing infrastructure, and translational life sciences have fostered a highly integrated research ecosystem. Within this landscape, Singapore-based research groups have made notable scientific contributions to the design and manufacture of customizable biological constructs, from engineered tissues and therapeutic cell systems to hybrid bio-devices and bio-interfaces.

Recently, advances in biomaterials science and AM have expanded the scope and sophistication of biofabrication. Platforms such as electrospinning [1], three-dimensional (3D) bioprinting [2], and metal AM [3] are enabling the fabrication of multilateral architectures with precisely tailored mechanical, biochemical, and structural properties. These technologies provide fine control over spatial organization and microenvironmental cues that are critical for applications in tissue engineering, soft bioelectronics, and functional food design [4–6]. Concurrently, integrating artificial intelligence (AI), machine learning (ML), and digital twin frameworks is transforming biomanufacturing from predominantly empirical, trial-and-error processes into predictive, data-driven production systems [7, 8]. These digital approaches support rational material design, real-time process monitoring, and closed-loop quality control, laying the foundation for robust, automated biofabrication pipelines.

Despite these technological advances, several scientific and translational challenges limit widespread adoption. Designing

biomaterials that simultaneously demonstrate adequate mechanical performance, biological functionality, sustainability, and manufacturability remains a major bottleneck [9]. Achieving reproducibility across fabrication platforms requires standardized processes, advanced sensing modalities, and integrated feedback control systems. Furthermore, industrial scalability is constrained by regulatory considerations, manufacturing costs, and inherent biological variability. Addressing these challenges is critical for achieving reliable, sustainable, and economically viable biomanufacturing systems. In Singapore, these issues are actively being addressed via interdisciplinary research programs that integrate materials science, digital manufacturing, and translational research, reinforcing the country's growing role within the global biofabrication and biomanufacturing landscape.

Recent regional reviews have highlighted the rapid progress in biomanufacturing and biofabrication across major research hubs worldwide [10–13]. China has emphasized the translation of 3D bioprinting for organ regeneration alongside regulatory and quality-control framework development [10]. Meanwhile, research in the UK and Ireland has focused on integrating biofabrication with sustainability, ethical governance, and healthcare system requirements [11]. Japanese studies have highlighted advances in biomaterials, 3D bioprinting, and interdisciplinary biomedical applications within the broader context of "Biomanufacturing 4.0" [12], whereas work from Israel has demonstrated innovations in peptide-based bio-inks, soft biohybrid systems, and industrial-scale biofabrication [13].

Against this global backdrop, this review highlights research by Singapore-based investigators across the interconnected domains of biofabrication and biomanufacturing. We first examine advances in sustainable biomaterials that support environmentally responsible and functional biofabrication. We then discuss enabling manufacturing technologies, including electrospinning, 3D bioprinting, and metal AM, which are reshaping fabrication capabilities. Finally, we review emerging applications, including AI/ML-assisted intelligent manufacturing, regenerative cell therapies, microneedle systems, food biomanufacturing, and bioelectronics. This review offers a perspective on how Singapore-based research integrates sustainable materials, advanced manufacturing platforms, and digital technologies to develop scalable, intelligent biofabrication systems that address global biomedical, nutritional, and industrial needs.

2 Sustainable biomaterials

Biomass waste valorization into functional biomaterials has become a central theme in sustainable biomanufacturing, reflecting growing global interest in circular material economies and environmentally responsible resource use [14]. As biomanufacturing progresses toward integrated, large-scale production systems, there is increasing demand for sustainable biomaterials that can be processed under mild conditions, tailored for specific biological functions, and engineered into advanced architectures. Within this landscape, researchers in Singapore have substantially contributed to the development of sustainable materials derived from a variety of biomass sources, including human hair keratin, aquaculture side-streams, plant-derived polysaccharides, and pollen, which offer abundant, low-cost, renewable feedstocks with intrinsic structural and biochemical advantages. These materials not only divert significant waste streams away from disposal but also provide versatile molecular building blocks that can be assembled into hydrogels, fibers, porous scaffolds, and microgels for downstream biomanufacturing applications. This section focuses on Singapore-led advances in biomass-derived biomaterial extraction, processing, and functionalization, highlighting their sustainability attributes, physicochemical performance, and potential to facilitate next-generation biomanufacturing.

2.1 Human hair keratin

Among waste-derived biomaterials, human hair keratin (HHK) is a unique resource due to its global abundance (>300,000 tons annually) and lack of established recycling pathways [15, 16]. Keratins extracted from human hair consist of fibrous proteins (~45–50 kDa) containing the leucine-aspartic acid-valine (LDV) amino acid motif, which confers intrinsic cell adhesion via integrin α4β1 recognition. The high cysteine content provides abundant free thiol groups, enabling diverse chemical modifications and crosslinking chemistries that confer HHK with substantial structural and functional versatility.

A simple yet effective approach to harnessing HHK is pH-induced precipitation, in which keratin self-assembles into hydrogel networks stabilized by disulfide exchange and hydrogen bonding. These hydrogel networks are cytocompatible, supporting in vitro fibroblast adhesion and proliferation while eliciting a minimal in vivo inflammatory response (Fig. 1a) [17, 18]. The naturally occurring high cysteine content in HHK enables gelation via metal-thiolate complexation. Silver ion ionic diffusion into HHK through a partially permeable membrane results in a hydrogel with a porosity gradient (Fig. 1b) [19]. Composites made with HHK have expanded utility; for example, HHK-alginate composites formed via amide coupling have exhibited favorable biocompatibility in subcutaneous implantation studies (Fig. 1c) [20] and have accelerated partial-thickness burn wound healing in porcine models [21].

Advanced structuring strategies have enabled increasingly sophisticated keratin architectures. Thiol-norbornene "click" reactions can produce cytocompatible photo-crosslinking of

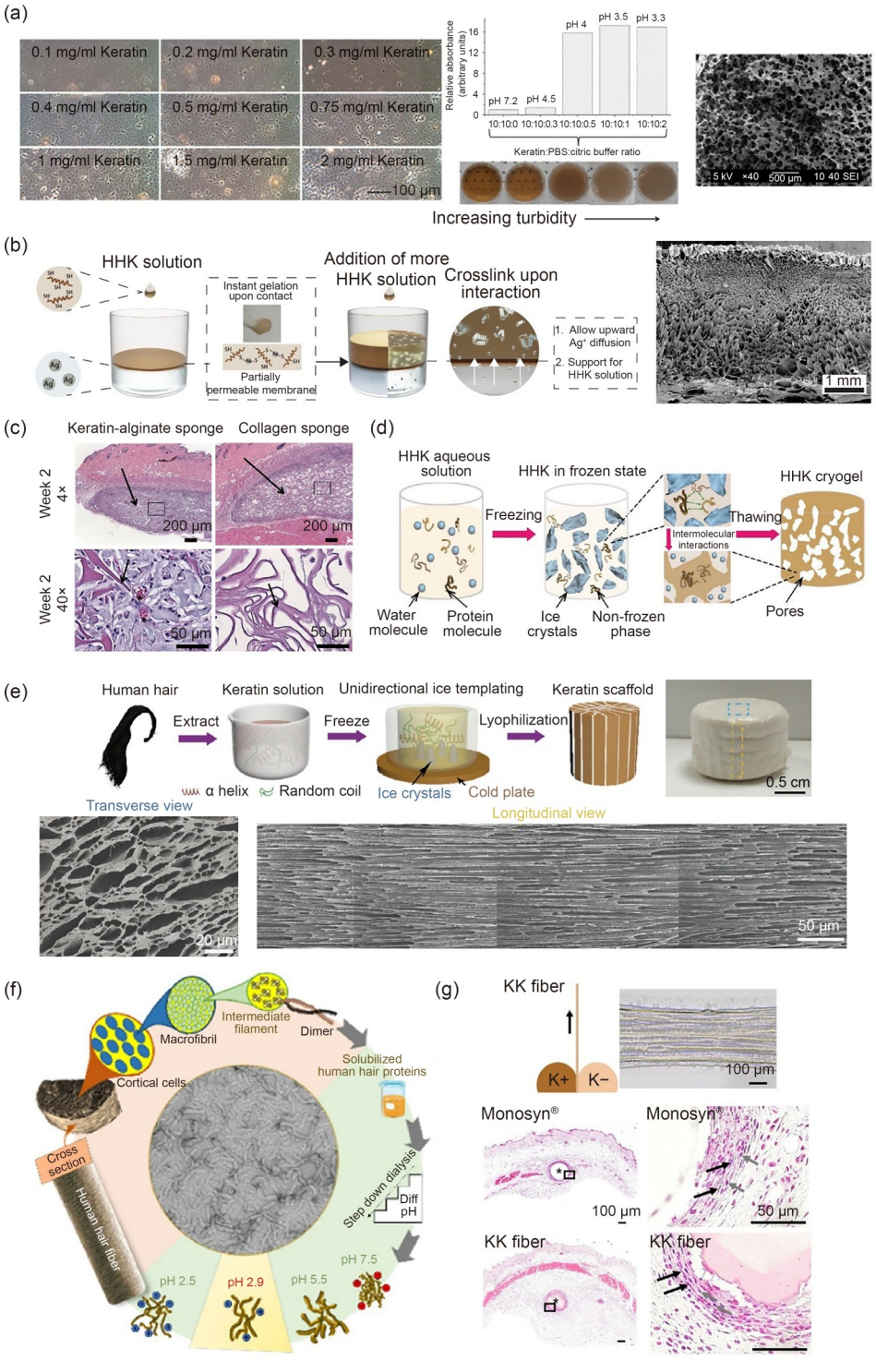

Fig. 1 Biofabrication with HHKs. (a) HHK hydrogel formed via pH-induced precipitation and stabilization. Reproduced from [18], with permission from the American Chemical Society. (b) HHK diffusion-mediated gradient gelation with silver ions forms hydrogels with porosity gradients. Reproduced from [19], licensed under CC-BY-NC-ND. (c) Subcutaneous implantation of a biocompatible HHK-alginate sponge. Reproduced from [20], with permission from John Wiley & Sons, Ltd. (d) Cryogelation of HHKs via repeated freeze-thaw cycles to form scaffolds with a well-connected pore network. Reproduced from [23], with permission from Wiley-VCH GmbH. (e) HHK scaffolds fabricated via the directed ice templating method possess anisotropic microarchitecture. Reproduced from [24], with permission from Wiley-VCH GmbH. (f) In vitro HHK self-assembly into a nanofibrous network through step-down dialysis in acidic buffer conditions (pH 2.9). Reproduced from [26], with permission from the American Chemical Society. (g) HHK fiber formation using interfacial polyelectrolyte complexation (IPC), with potential application as medical sutures. Asterisks indicate the original position of the suture material, whereas black rectangles indicate the region of interest shown in higher magnification hematoxylin and eosin images. Black arrows point to fibroblasts, and gray arrows point to neutrophils. Reproduced from [27], with permission from Elsevier Ltd.

keratin-polyethylene glycol composites, supporting precise spatial patterning [22]. Cryogelation via controlled thiol oxidation produces robust scaffolds with tunable mechanical properties (Fig. 1d) [23], whereas directional ice templating yields anisotropic porous keratin networks with aligned microarchitectures mimicking native fibrous tissues (Fig. 1e) [24]. Reinforcement with polydopamine enhances strain-stiffening behavior, a key requirement for soft tissue mimicry [24, 25]. Keratin can also self-assemble into intermediate filament-like nanostructures under step-down dialysis (Fig. 1f) [26], and interfacial polyelectrolyte complexation (IPC) facilitates the fabrication of keratin microfibers that perform comparably to commercial sutures (Fig. 1g) [27].

Collectively, these diverse keratin-based technologies illustrate how an abundant and underutilized waste stream can be transformed into a high-performance, structurally versatile biomaterial platform. Keratin's broad processability (from simple hydrogels to engineered microporous networks) positions it as an upstream material compatible with multiple biofabrication techniques. A practical consideration for making keratin valorization commercially viable is cost-effectiveness within a circular-economy framework, which begins with selecting chemicals for extraction. Using expensive reducing agents such as dithiothreitol, although effective, increases the cost of producing usable keratin on a large scale. Transitioning away from urea-based reductive extraction methods, cheaper alternatives such as deep eutectic solvents have been explored [28, 29], leading to a significant reduction in the cost of extracted keratin [30]. Exploring greener, lower-cost extraction methods to obtain keratins suitable for biofabrication will be essential moving forward.

2.2 Valorizing aquaculture side-streams

Aquaculture, one of the fastest-growing food sectors worldwide, generates large volumes of underutilized byproducts, such as fish skin, scales, and bones. These side-streams are naturally rich in collagen, minerals, and extracellular matrix (ECM) components, offering an abundant, ethical, and non-mammalian alternative to bovine or porcine sources. Their upcycling not only reduces environmental burden but also allows the development of sustainable biomaterials for regenerative medicine, including scaffolds, hydrogels, and advanced tissue-engineering constructs.

Despite their strong potential, aquaculture-derived side-streams are influenced by biological variability and seasonal fluctuations, which affect collagen yield and composition and downstream material performance. This variability presents challenges for reproducibility, standardization, and regulatory translation. However, the rapid expansion of inland fisheries has significantly reduced these constraints by providing tighter control over species selection, diet, growth conditions, and harvesting schedules [31]. Integration with established tilapia farming within local fishing industries provides a stable, traceable supply of raw material, reducing dependence on wild-caught fish and improving resilience to the supply-chain disruptions commonly associated with marine harvesting.

Within this context, tilapia skin has emerged as a highly valuable feedstock due to its high type I collagen content and well-preserved ECM architecture. Through enzymatic epidermal removal followed by sodium dodecyl sulfate (SDS)-mediated decellularization, nuclease treatment, and freeze-drying, tilapia skin can be converted into decellularized tilapia skin (DTS) scaffolds that retain native collagen organization and mechanical integrity [32]. DTS has a high denaturation temperature (~68 °C), a favorable Young's modulus (~56 MPa), and slow degradation kinetics, making it particularly suitable for load-bearing tissue repair. Parallel extraction of collagen from tilapia skin with acid solubilization enabled the fabrication of electrospun collagen nanofibers that, once crosslinked, promoted osteoblast adhesion, mineralization, and bone regeneration in rat calvarial defect models [32].

Building on these advances, acid-solubilized tilapia collagen has also been developed as a platform material for engineered human skin equivalents (HSEs). Collagen is extracted through a controlled sequence of descaling, alkaline pretreatment to remove noncollagenous proteins, fat extraction with butanol, and solubilization in acetic acid, followed by NaCl-induced precipitation, redissolution, dialysis, and lyophilization [33]. This method yields a high-purity (~100%) collagen product with an extraction efficiency of (42±1)%. Although fish collagen preserves the molecular attributes of mammalian collagen, its lower thermal stability and softer mechanical properties typically require reformulation before it can serve as a robust scaffold material. To overcome these limitations, collagen has been blended with fibrin to create fortified fish collagen (FFC), a hydrogel that enhances matrix stability while avoiding the cytotoxicity associated with chemical crosslinkers. The optimized formulation (3 mg/mL collagen + 0.5 mg/mL fibrin) resists fibroblast-induced contraction and retains the triple-helical structure of collagen [33]. FFC also benefits from a high amino acid content (199/1000 residues), conferring a favorable denaturation temperature (39.4 °C) comparable to mammalian collagen. As a dermal matrix for full-thickness HSEs, FFC supports dermal fibroblast and epidermal keratinocyte attachment and proliferation, enabling the formation of biomimetic bilayered skin constructs (Fig. 2a). These HSEs exhibit excellent barrier integrity, demonstrated by the highest transepithelial electrical resistance among tested skin models. Additionally, the platform is readily adaptable to high-throughput 96-well formats, reducing reagent and cell consumption tenfold.

A complementary valorization approach has addressed the intrinsic instability of pure fish collagen hydrogels by engineering a piezoelectric composite hydrogel (Col/oxidized

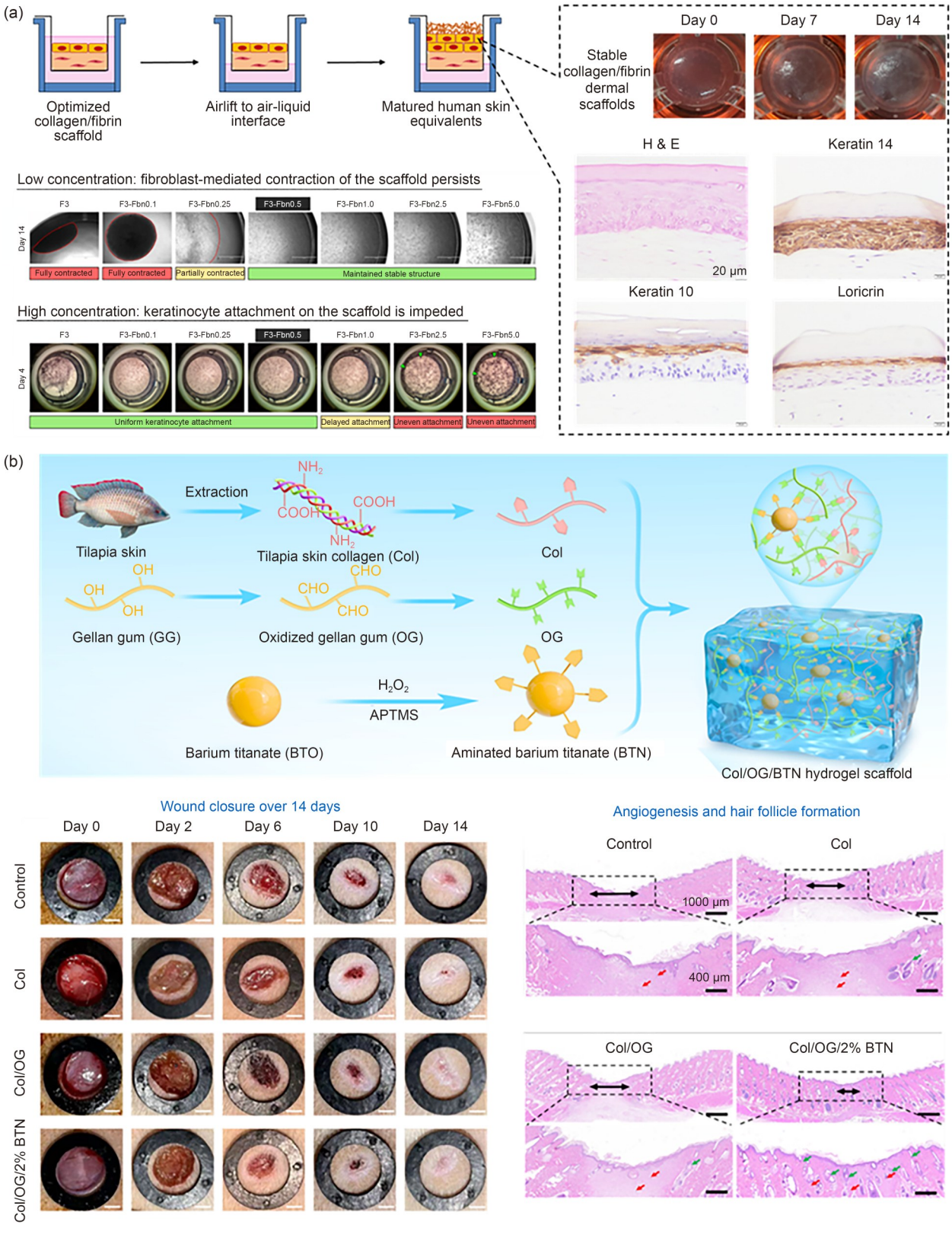

Fig. 2 Biofabrication using aquaculture byproducts, such as tilapia skin. (a) A stable dermal scaffold was constructed by optimizing a combination of collagen and fibrin, generating 3D human skin equivalents. Reproduced from [33], with permission from Elsevier B.V. (b) A piezoelectric hydrogel scaffold was developed based on barium titanate-encapsulated tilapia-skin-derived collagen and oxidized gellan gum. When applied to a rat wound model, the scaffold promoted wound healing by immune modulation, enhanced angiogenesis, and increased collagen deposition. Reproduced from [34], licensed under CC-BY-NC-ND

gellan gum (OG)/barium titanate nanoparticles (BTNs)) for advanced wound healing applications [34]. For this purpose, tilapia collagen is incorporated into a dual-network scaffold with OG and amino-modified BTNs. Schiff-base crosslinking between OG aldehyde groups and collagen amines establishes the primary network; further crosslinking via BTN's amine group conjugation to OG aldehyde groups imparts a hierarchical structure, mechanical reinforcement, and piezoelectric responsiveness. The resulting hydrogel features a highly porous, hydrophilic 3D architecture with a compressive modulus of 8–18 kPa, like that of native skin. An enhanced hydroxyproline content and dual-network stabilization raise the denaturation temperature to 47.1 °C and improve biodegradation control. Importantly, the scaffold functions as a wireless, ultrasound-activated piezoelectric material (with a piezoelectric coefficient of 18.5 pC/N) that converts mechanical stimulation into bioelectrical cues. In vivo, these signals shift macrophages from pro-inflammatory M1 to regenerative M2 phenotypes while promoting angiogenesis via phosphoinositide 3-kinase (PI3K)/Akt activation and tumor necrosis factor (TNF) pathway suppression. This mechanobiologically active environment accelerates wound closure, enhances collagen organization, and supports hair follicle regeneration, achieving high-quality skin repair (Fig. 2b).

In addition to tilapia-derived biomaterials, integrated valorization strategies are exploiting other aquaculture sidestreams. For example, collagen from American bullfrog skin can be combined with hydroxyapatite (HAp) extracted from calcined snakehead fish scales [35]. Collagen is obtained via a mechano-chemical process encompassing homogenization, alkaline deproteinization, acid solubilization, salt precipitation, dialysis, and lyophilization; HAp is produced by thermally converting the calcium-rich matrix of fish scales at 850 °C into highly crystalline ceramic particles. When blended and crosslinked, the resulting composite scaffolds exhibited >90% porosity with ~55 μm pores, supporting osteoblast adhesion, osteogenic gene expression, and mineral deposition. These studies highlight the versatility of aquaculture biomass as a renewable and scalable feedstock for producing bioactive, structurally robust materials for both soft- and hard-tissue engineering applications.

2.3 Plant-derived polysaccharides

Plant biomass provides renewable, nontoxic polysaccharides that can be chemically modified to produce functional hydrogels for biomedical applications. Flaxseed gum (FG), a water-soluble heteropolysaccharide extracted from a widely cultivated crop, has attracted considerable attention due to its biocompatibility and scalability [36]. Using an aqueous methacrylation process with methacrylic anhydride followed by extensive dialysis, FG can be converted into methacrylated flaxseed gum (FGMA), a photo-crosslinkable derivative prepared without organic solvents. This workflow minimizes chemical waste and yields a purified polymer suitable for use under physiological conditions.

FGMA hydrogels display impressive mechanical resilience, including fatigue resistance under cyclical loading and prolonged degradation over approximately 66 d. Their viscoelastic properties can be customized by adjusting the concentration and degree of substitution, enabling the design of matrices with stiffness profiles tailored to different tissue environments. In osteochondral regeneration models, FGMA-based constructs support mesenchymal stem cell viability and promote differentiation toward chondrogenic lineages, leading to cartilage repair outcomes comparable to those of native tissue. These findings indicate that FGMA can serve as a robust, bioactive, and mechanically competent hydrogel system for load-bearing soft tissue applications.

Importantly, FGMA demonstrates how plant-derived polysaccharides can be transformed into high-performance biomaterials using green, water-based chemistries. Its renewable origin, food-safe nature, and scalable production make it a compelling example of a sustainable polysaccharide platform that can be integrated into diverse biomanufacturing workflows.

2.4 Expanding landscape of sustainable biomass-derived biomaterials

Across these examples, a unifying principle is that biomass, commonly regarded as waste, can be transformed into high-value biomaterials suitable for advanced biomanufacturing. These systems share common sustainability features, including resource circularity, reliance on abundant feedstocks, mild aqueous processing conditions, and reduced dependence on synthetic reagents. Their intrinsic biocompatibility and structural tunability facilitate seamless integration into downstream fabrication technologies, including hydrogel formation, microfabrication, fiber production, and scaffold engineering. Collectively, sustainable biomaterials lay the upstream foundation for next-generation biomanufacturing.

3 Biofabrication technologies

Advances in biofabrication have enabled biological construct production across nano-, micro-, and macro-scales, supporting increasingly sophisticated applications in tissue engineering and regenerative medicine. Among the diverse technological platforms available, electrospinning, 3D bioprinting, and metal AM form a complementary toolkit enabling precise control over architecture, composition, and cellular organization. In this section, we examine critical advances across these technologies with a particular emphasis on research conducted by the biomanufacturing community

in Singapore, whose efforts reflect the nation's broader strategic focus on advanced manufacturing, sustainability, and translational biomedical innovation. By summarizing these Singapore-led studies, this section highlights their scientific contributions to material processing, printing physics, and application-driven design.

3.1 Electrospinning

Electrospinning is a versatile, widely adopted technique for producing nanofibrous scaffolds. It remains a cornerstone of soft-material biomanufacturing. In this process, a high-voltage electric field is applied to a polymer solution, inducing the elongation of a charged polymer droplet into a fine liquid jet. As the jet accelerates, a Taylor cone forms at the spinneret tip, and solvent evaporation solidifies the polymer into continuous nanofibers [37]. The resulting fibers possess high surface area-to-volume ratios, tunable porosity, and nanoscale morphologies that closely resemble the ECM, making them highly conducive to cell adhesion, proliferation, and differentiation. Over the years, advancements such as coaxial, emulsion, and melt electrospinning have significantly expanded the design space of nanofibrous constructs, offering sophisticated material architectures for biomedical and biomanufacturing applications (Fig. 3) [38].

Electrospun nanofibers have gained substantial traction in drug delivery due to their ability to encapsulate bioactive compounds and modulate release profiles by controlling fiber geometry, porosity, and composition. Both natural and synthetic polymers, including sodium alginate [39], polyvinyl alcohol [40], and clay-reinforced nanocomposites [41], have been adapted for applications ranging from transdermal drug delivery to the controlled release of chemotherapeutic agents. More recently, integrating stimuli-responsive chemistries with electrospun matrices has enabled the development of "intelligent" nanofiber systems capable of pH-responsive drug release with near-infrared real-time monitoring, representing a notable step toward clinically adaptable, precision-controlled therapeutic platforms [42].

In tissue engineering, electrospinning has facilitated biomimetic scaffold fabrication for multiple organ systems. Arginylglycylaspartic acid (RGD)-functionalized nanofibers have promoted cardiomyocyte adhesion and maturation for cardiac repair [43], whereas aligned nanofiber constructs have guided endothelial cell organization in small-diameter vascular grafts [44]. Anti-calcification nanofibrous grafts demonstrate the potential for long-term vascular transplantation [45]. Additionally, conductive polymer nanofibers combined with electrical cues have accelerated nerve regeneration [46]. In hepatic applications, ECM-inspired nanofiber networks have sustained hepatocyte function within bioartificial liver systems, offering supportive platforms for end-stage liver disease [47]. Coaxial electrospinning further grants spatial control over bioactive factor incorporation, enhancing osteogenesis and chondrogenesis in bone and cartilage repair [48]. Parallel advances in wound dressings, including nanofiber systems loaded with anti-microbial agents [49], plant-derived bioactives [50, 51], or therapeutic polypeptides [52], address long-standing challenges in chronic wound management and antimicrobial resistance.

The utility of electrospinning extends beyond regenerative scaffolds into the realm of wearable and implantable biomedical devices. The intrinsic flexibility, conductivity, and

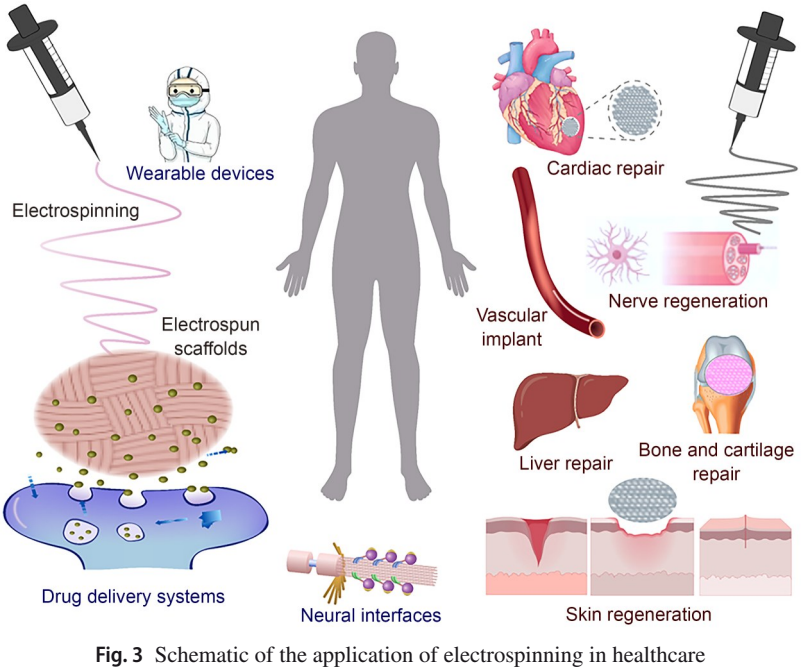

Fig. 3 Schematic of the application of electrospinning in healthcare

biocompatibility of nanofibrous materials have enabled applications such as Janus nanofiber membranes for respiratory protection [53], pumpless sweat-sensing yarns for real-time glucose monitoring [54], and soft, conformable electrodes for continuous physiological monitoring and human–machine interfacing [55]. In neural engineering, electrospun conductive nanocomposites have enabled the development of biocompatible neural interfaces with high signal fidelity [56], advancing the potential of neuroprosthetics and brain–machine communication.

Together, these developments highlight the breadth and adaptability of electrospinning as a biomanufacturing platform. Its unique ability to generate biomimetic, functionally customizable nanostructures supports a wide variety of applications from drug delivery and regenerative medicine to wearable systems and neural technologies. As innovations in responsive nanofibers, hybrid composites, and integrated sensing continue to develop, electrospinning is poised to become a foundational technique within modern biomanufacturing and a key driver of translational soft-material technologies.

3.2 3D bioprinting

3D bioprinting provides the spatially controlled placement of cells, biomaterials, and biochemical cues to generate architecturally complex and biologically functional constructs. Depending on their underlying deposition mechanism, bioprinting technologies are broadly classified into extrusion-based, jetting-based, and vat photopolymerization-based systems, each offering distinct advantages in terms of printing resolution, the range of bio-ink viscosities that can be printed, and cell-processing conditions. These modalities impose different requirements on bio-ink rheology, crosslinking kinetics, and process stability, making the interplay between material design and printing physics a central focus of ongoing research. In this subsection, we highlight selected recent advances in extrusion, jetting, and vat photopolymerization bioprinting, based on studies conducted by researchers in Singapore, and illustrate their scientific contributions to improved print fidelity, enhanced cell viability, and the broader translational potential of 3D bioprinting technologies.

3.2.1 Extrusion-based bioprinting

Extrusion-based bioprinting is widely used to fabricate cell-laden constructs based on its compatibility with hydrogels across a broad viscosity range and its ability to produce clinically relevant, centimeter-scale architectures. Achieving high-fidelity printing requires bio-inks with finely tuned rheological properties (most notably shear-thinning behavior, adequate yield stress, and rapid structural recovery) combined with crosslinking strategies that stabilize deposited filaments while preserving cell viability. Recent progress in the field reflects concurrent advances in bio-ink formulation, support-bath strategies, computational modeling of printing physics, and the production of structurally complex, functionally graded tissues, such as osteochondral and cartilage constructs.

A key development in bio-ink design is the emergence of physically crosslinked gelatin-based bio-inks, which eliminates the requirement for photo-initiators or chemical crosslinkers while maintaining robust printability. Gelatin formulated with gellan gum and nanosilicate Laponite XLG (Gel-X) forms a reinforced network stabilized via polyelectrolyte complexation and physical interactions (Fig. 4a) [57]. This noncovalent network provides pronounced shear-thinning properties, rapid viscoelastic recovery, and improved dimensional stability compared to conventional gelatin hydrogels, while also slowing degradation under physiological conditions. The ability of these physically crosslinked bio-inks to maintain high cell viability during extended culture exemplifies that noncovalent networks can provide both structural fidelity and biological compatibility for extrusion-based bioprinting.

To address the limitations associated with low-viscosity bio-inks, particularly filament collapse, support bath-assisted approaches have been developed. In these approaches, a thixotropic alginate/methylcellulose (Alg/MC) hydrogel functions as either a co-printed support or as a supporting matrix into which gelatin methacrylate (GelMA) is directly extruded [58]. Electrostatic interactions between the positively charged GelMA and polyanionic Alg/MC enhance interfacial cohesion, whereas the surrounding support matrix confers geometric stability during printing. A single postprinting ultraviolet (UV) exposure step then stabilizes the GelMA phase, reducing the cumulative phototoxicity associated with repeated curing. This strategy enables the fabrication of intricately shaped, multicellular constructs with high structural fidelity and cell viability exceeding 93%. Expansion of this concept has led to dual-crosslinkable bio-inks integrating a temperature-dependent physical network with a secondary UV-induced covalent network (Fig. 4b). These systems leverage complementary sol–gel transitions, such as between GelMA and methylcellulose derivatives, to provide yield stress and self-healing behavior at physiological temperatures, followed by photopolymerization for long-term mechanical stability [59]. These dual-network bio-inks support the embedded bioprinting of perfusable channels and large hydrogel volumes at 37 °C, while maintaining cell viabilities >90%, addressing a key limitation of conventional single-network GelMA bio-inks.

In addition to polymeric networks, natural particulate systems, like pollen-derived microgels, have expanded the design space for extrusion bio-inks. Through an aqueous alkaline swelling process, rigid sunflower pollen grains can be converted into monodisperse microgels that exhibit viscoplasticity and shear-thinning behavior suitable for the rheological modification of composite bio-inks [60]. When incorporated

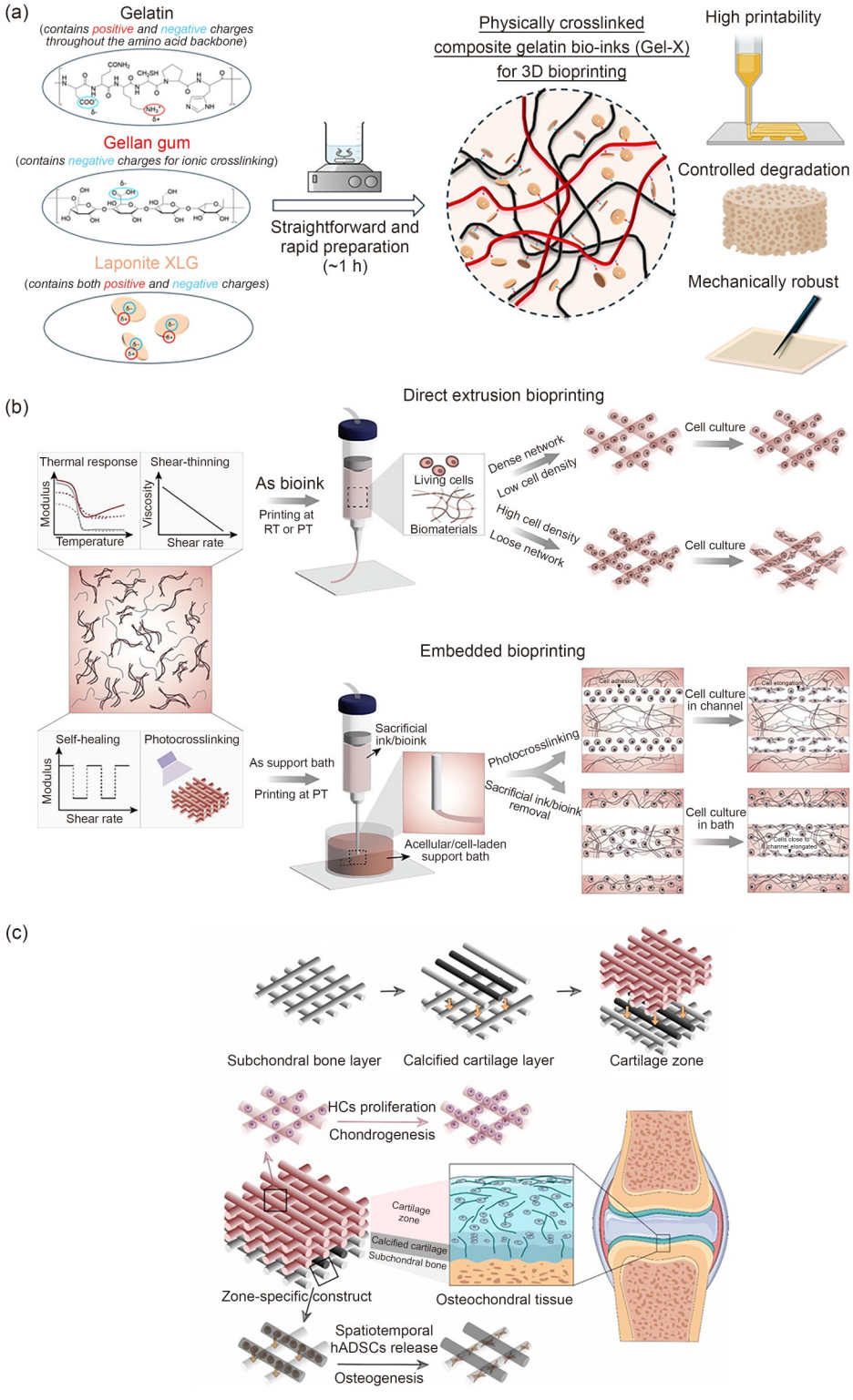

Fig. 4 Extrusion-based bioprinting. (a) Physically crosslinked bio-ink (Gel-X) comprising gelatin, gellan gum, and Laponite XLG allows multimodal 3D bioprinting. Prepared within 1 h by simple mixing in deionized water, Gel-X offers improved printability, mechanical strength, and long-term structural stability under physiological conditions. Reproduced from [57], licensed under CC BY 4.0. (b) Schematic of a dual photo- and thermo-crosslinkable bio-ink designed for direct extrusion and for use as a support bath for embedded 3D bioprinting. Reproduced from [59], with permission from Elsevier Ltd. (c) One-step hybrid 3D printing of an osteochondral triphasic construct: a PCL/TCP-printed subchondral bone layer; a calcified cartilage layer co-printed with GelMA/human adipose-derived stem cells (hADSCs) and PCL/TCP for hADSC release and bone-layer attachment; a cartilage layer printed using MCMA/GelMA/HCs to preserve the chondrocyte phenotype. Reproduced from [62], licensed under CC BY 4.0. PCL: polycaprolactone; TCP: tricalcium phosphate; MCMA: methacrylated methylcellulose; HCs: human chondrocytes

into alginate-based or hyaluronic acid-based formulations, pollen microgels enhance mechanical robustness, improve print fidelity, and introduce pH-responsive properties. Concentrated microgel suspensions can also serve as reusable support matrices for support bath-assisted bioprinting, enabling the generation of highly complex structures. Their natural abundance, sustainable origin, and mild processing requirements make pollen microgels an appealing class of biofabrication additives.

Advances in extrusion bioprinting extend beyond ink chemistry to include process-level optimization of the print-head. Computational fluid dynamics (CFD) has been applied to evaluate the flow behavior, mixing efficiency, and shear profiles within multimaterial print-head geometries [61]. These simulations have provided mechanistic insight into how nozzle design, flow rate, and shear-thinning rheology influence velocity distributions and wall shear stress. Additionally, they predict outlet conditions that minimize cell-damaging stresses, while ensuring homogeneous material composition. Such modeling tools enable the rational optimization of internal mixing chambers and coextrusion pathways, supporting hardware design that balances material uniformity, structural fidelity, and cell protection.

The convergence of ink engineering and process control has enabled the production of functionally graded tissue constructs, including biomimetic osteochondral grafts. Hybrid bioprinting strategies combining soft hydrogel-based bio-inks with bioceramic-reinforced thermoplastics have enabled the creation of triphasic constructs that reproduce the zonal architecture of native osteochondral tissues (Fig. 4c) [62]. In these systems, hydrogel regions recapitulate chondrogenic microenvironments, whereas composite polycaprolactone (PCL)/tricalcium phosphate (TCP) layers provide bone-like mechanical reinforcement and promote integration with mineralized tissues. Encapsulated stem cells and chondrocytes respond to these printed microenvironments with zone-specific behaviors, including directed migration, appropriate matrix deposition, and maintenance of chondrogenic phenotypes, underscoring the biological relevance of such engineered architectures.

Sustainably sourced polysaccharide-based inks have also strengthened the capabilities of extrusion-based bioprinting for cartilage applications. FGMA, produced via aqueous-phase methacrylation, yields high-strength bio-inks with a compressive modulus up to 41-fold higher than GelMA and high fatigue resistance under cyclic loading [36]. These inks maintain favorable shear-thinning behavior for printing, exhibit slow degradation over roughly 66 d, and provide mechanical integrity suitable for load-bearing cartilage applications. When printed with mesenchymal stem cells, FGMA constructs promote lineage-specific differentiation and form neocartilage with structural and functional properties comparable to those of native tissue.

Overall, advancements in extrusion-based bioprinting highlight the field's multifaceted progression. Modern bio-inks integrate physical and covalent crosslinking mechanisms, sustainable microgel additives, and reinforced polymer networks. Support-bath strategies have enabled the direct printing of complex geometries, and CFD-guided print-head optimization improves material uniformity and reduces cellular stress. Combined with application-driven construct design, these developments have yielded structurally and biologically relevant osteochondral and cartilage tissues. Collectively, they establish extrusion-based bioprinting as a versatile and increasingly mature platform for producing high-fidelity, mechanically customizable, clinically meaningful tissue-scale constructs.

3.2.2 Jetting-based bioprinting

Jetting-based bioprinting is a contactless drop-on-demand (DOD) technology that dispenses subnanoliter droplets with high spatial precision, enabling the controlled patterning of cells, biomolecules, and bio-inks in a highly automated manner [63]. This modality encompasses a broad spectrum of actuation mechanisms, including inkjet printing, microvalve-based dispensing, acoustic bioprinting, laser-induced forward transfer, and electrohydrodynamic jetting, each offering distinct advantages for achievable resolution, printable viscosity range, and ease of operation [64]. Together, these jetting-based approaches offer versatile platforms for fabricating finely patterned biological constructs across multiple application domains. This subsection highlights key advances in bio-ink formulation, droplet physics, and application-driven printing strategies, underscoring the evolving capabilities of jetting-based bioprinting.

Bio-ink formulation strategies remain central for enhancing both printability and cytocompatibility. One notable approach involves modifying GelMA-based bio-inks to permit reliable ejection during thermal inkjet (TIJ) bioprinting. A two-step process combining saponification and controlled heat treatment yields heat-treated saponified GelMA (HSP-GelMA), which undergoes a substantial reduction in molecular weight (from ~224.3 to ~31.6 kDa) and viscosity (from ~17.6 to ~3–4 mPa·s) after two autoclave cycles, supporting stable droplet formation in commercial print-heads [65]. Importantly, despite reduced functionalization, HSP-GelMA retains its ability to undergo physical gelation and UV-induced chemical crosslinking, enabling high cell viability and proliferation postprinting. However, excessive heat exposure compromises its photo-crosslinkability and mechanical integrity, highlighting the need to carefully balance viscosity reduction with structural robustness. Complementary work on polyvinylpyrrolidone (PVP)-based formulations has demonstrated how polymer additives can modulate viscosity, surface tension, and viscoelastic behavior to improve jet stability and suppress satellite formation [66]. These PVP-enhanced

inks also support robust fibroblast proliferation, highlighting their suitability for applications that require both print fidelity and cell-friendly matrix environments. Collectively, these studies establish a growing library of bio-inks optimized for the unique rheological and functional requirements of jetting-based bioprinting.

Beyond bulk hydrogel inks, cell-laden hydrogel microparticle (HMP) development has introduced a modular, highly customizable approach to tissue assembly. Using TIJ deposition into a surfactant-stabilized water-in-oil emulsion, subnanoliter droplets of GelMA-based formulations can be rapidly coalesced and UV-crosslinked to form HMPs with diameters from ~30 μm to >500 μm [67]. Surfactant concentration governs the interfacial stability and droplet coalescence, whereas the biocompatible TIJ process preserves ~76% cell viability. The platform also enables multimaterial encapsulation, allowing heterogeneous cell types or biomolecules to be patterned within single microparticles. These attributes position TIJ-mediated HMP fabrication as a high-throughput, flexible strategy for producing building blocks for granular bio-inks or supporting bath matrices.

Parallel efforts in process optimization have advanced our fundamental understanding of droplet physics and its implications for cell survival. Systematic studies have revealed that both droplet impact velocity and droplet volume are critical determinants of cell viability [68]. High-speed imaging revealed that increasing the cell concentration from 1 million to 4 million cells/mL increased bio-ink viscosity and reduced impact velocity to ~5.77 m/s, significantly limiting impact-induced mechanical injury. Time-resolved imaging further demonstrated that small droplets (20 nL) evaporated far more rapidly than larger droplets (40 nL), resulting in hypertonic microenvironments that reduced the cell viability from (88.3± 2.45)% to (48.2±3.54)% within 4 min; all droplets fell below 50% viability by 6 min due to severe evaporation stress. These findings reveal a delicate balance between resolution (favored by small droplets) and cytocompatibility (favored by larger droplets). Consequently, maintaining droplet volumes ⩾20 nL and limiting printing durations to <2 min for 20–30 nL droplets (and <4 min for 40 nL droplets) is recommended to preserve cell viability >85%. Jetting-based bioprinting under these optimized conditions supports fibroblast proliferation to ~90% confluence by Day 7, confirming that careful control of droplet impact velocity and evaporation dynamics is essential for ensuring both immediate and long-term cell function. These insights provide quantitative guidelines for achieving high-precision cell-laden droplet printing.

Finally, advances in jetting modalities have broadened the scope of bioprinting applications, particularly for thin, multilayered, and physiologically structured tissues. In bioprinted human alveolar lung models, jetting-based deposition offers a precise spatial arrangement of epithelial, stromal, and endothelial cells to recreate the delicate multilayered organization of the alveolar interface [69]. These constructs display appropriate barrier formation and cell–cell organization, demonstrating the ability of inkjet printing to recapitulate complex microenvironments. Similarly, layered deposition of human keratinocytes, melanocytes, and fibroblasts has produced pigmented human skin constructs with uniform pigmentation and physiologically relevant epidermal stratification [70]. These studies highlight the precision with which jetting platforms can orchestrate multicellular spatial organization, a key requirement for dermatological and cosmetic applications.

The stringent ink requirements of jetting-based systems have traditionally constrained the types of bio-inks that can be reliably printed. However, recent innovations in viscosity-reduced GelMA derivatives and PVP-enhanced formulations to modular HMPs have substantially widened the material space compatible with DOD actuation. Meanwhile, deeper insights into droplet formation dynamics, impact mechanics, and evaporation-induced cell stress have enabled rational printing parameter tuning to enhance both jetting fidelity and cytocompatibility. These material and process advances, together with successful demonstrations in retinal, pulmonary, and skin tissue models, highlight the growing capability of jetting-based bioprinting to produce multicellular, multilayered, thin tissue constructs that benefit from high spatial precision.

3.2.3 Vat photopolymerization-based bioprinting

Vat photopolymerization encompasses stereolithography (SLA), digital light processing (DLP), and related light-based bioprinting techniques in which photo-crosslinkable bio-inks are polymerized layer by layer using controlled light exposure [71, 72]. In contrast to extrusion and jetting systems that rely on mechanical dispensing, vat photopolymerization provides high spatial resolution (~30 μm), rapid fabrication speeds, and negligible shear stress on encapsulated cells. These attributes make vat photopolymerization-based bioprinting especially suited for constructing high-resolution microarchitectures, such as perfusable microchannels, vasculature-inspired networks, and neural guidance structures, in which geometric precision and mechanical fidelity are critical. Recent developments have focused on engineering photo-crosslinkable bio-inks with improved mechanical and biological performance, expanding process-level control over spatial heterogeneity, and demonstrating application-specific tissue constructs leveraging the unique capabilities of vat-based platforms.

Significant advancements have been made in engineering composite bio-inks that balance structural robustness with cytocompatibility. One key development involves the use of poly(ethylene glycol) dimethacrylate (PEGDMA; $M_W \approx$ 1 kDa) as a more accessible and biocompatible alternative to high-molecular-weight poly(ethylene-glycol)-diacrylate

(PEGDA) in SLA bioprinting [73]. GelMA alone offers limited shape fidelity at room temperature and requires high polymer concentrations for stable printing, whereas PEGDMA incorporation significantly enhances the mechanical strength and dimensional stability of the resulting hydrogels without introducing the cytotoxicity commonly associated with short-chain PEGDA. Composite formulations containing 4% GelMA with 4%–15% PEGDMA generate constructs with customizable stiffness (~10–80 kPa) and excellent geometric accuracy, enabling the fabrication of overhangs, lattices, and other mechanically demanding features. These composites maintained high encapsulated-cell viability (71%–87% over 6 d), demonstrating their suitability for producing larger, cell-laden constructs via SLA while preserving biological function. That work exemplified how composite ink design can expand the material versatility and application range of vat photopolymerization-based bioprinting.

In addition to material formulation, recent work has demonstrated novel voxel-level control in the DLP system. A composable-gradient DLP strategy was introduced in which exposure dose and pixel-wise precursor solution mixing are independently modulated, enabling gradients in matrix stiffness, porosity, cell density, and material within a single construct (Fig. 5a) [74]. Critically, these gradients are generated without altering the underlying ink chemistry, relying instead on a microfluidic mixer to produce continuous or discrete gradients in real time. This tunable heterogeneity offers a powerful route to engineer functionally graded tissues and biomimetic interfaces.

The strengths of vat photopolymerization are further demonstrated by its use in neural microchannel fabrication. DLP printing of GelMA and GelMA-PEGDA bio-inks provides human induced pluripotent stem cell-derived spinal cord progenitor cell (SCPC) encapsulation within single-layer (2-mm thick) microchannel constructs, avoiding the shear stresses and prolonged build times associated with extrusion methods (Fig. 5b) [75]. The technique achieved highly resolved channels (~300 μm diameter) with neck-to-neck spacing as low as 50 μm. Moreover, the scaffold stiffness directed SCPC lineage specification: stiffer 10% GelMA scaffolds promoted motor neuron differentiation (~9.4%), whereas softer 7.5% GelMA scaffolds favored interneuron differentiation (~7.3%). These findings illustrate how vat photopolymerization-based bioprinting can integrate precise architectural control with biologically relevant mechanical cues to guide cell fate, highlighting its potential in neural tissue engineering and microphysiological model development (Figs. 5c–5g).

These advances highlight the growing utility of vat photopolymerization as a high-resolution biomanufacturing technology. Innovations in bio-ink engineering, such as PEGDMA-reinforced GelMA composites, along with pixel-level gradient control and successful demonstrations in neural tissue model fabrication, highlight the ability of vat photopolymerization-based bioprinting to achieve microscale architectural complexity and rapid fabrication. As photo-crosslinking chemistries continue to evolve and printing platforms become increasingly modular and programmable, vat photopolymerization is poised to play an essential role in producing architecturally sophisticated tissue constructs that require fine spatial control and finely tuned microenvironmental cues.

3.3 Metal additive manufacturing

Metal AM has become a critical pillar in biomanufacturing, especially for producing load-bearing, patient-specific implants that demand high mechanical strength, wear resistance, and long-term structural stability. In contrast to polymer-based biofabrication, metal AM enables the production of components with superior mechanical properties, making it indispensable for orthopedic, dental, and maxillofacial applications. Among the wide range of metallic biomaterials explored, both Mg and Ti alloys hold promise due to their biocompatibility, favorable mechanical behavior, and, for Mg, the ability to biodegrade in vivo. This subsection highlights recent advances in the AM of Mg and Ti alloys, with an emphasis on strategies that address the unique challenges associated with printing and translating these biomaterials.

3.3.1 Magnesium alloys

Mg alloys have emerged as attractive candidates for temporary, bioresorbable implants due to their biodegradability, biocompatibility, and mechanical properties that closely match those of cortical bone. These attributes allow Mg-based implants to gradually resorb as new tissue forms, eliminating the need for secondary removal surgeries. Despite these advantages, clinical translation remains constrained by several interrelated challenges, including controlling corrosion rates with suitable protective coatings, achieving adequate densification during processing, mitigating contamination, and balancing porosity with mechanical performance.

Among these factors, porosity is a critical design parameter for AM Mg scaffolds. Porous architectures enhance osteointegration, vascularization, and nutrient transport; however, increasing porosity inevitably compromises mechanical strength and accelerates corrosion. Binder jet printing (BJP) technology is particularly effective in enabling controlled porosity levels over a wide range. Studies on BJP-fabricated Mg–Zn–Zr scaffolds clearly illustrate this trade-off: increasing porosity from 13% to 27% results in 40%–70% reductions in tensile strength and 11%–30% reductions in compressive strength, alongside corrosion rates more than an order of magnitude higher than those of cast alloys [76]. These findings highlight the need to optimize pore architectures to retain biological functionality without sacrificing essential load-bearing capacity.

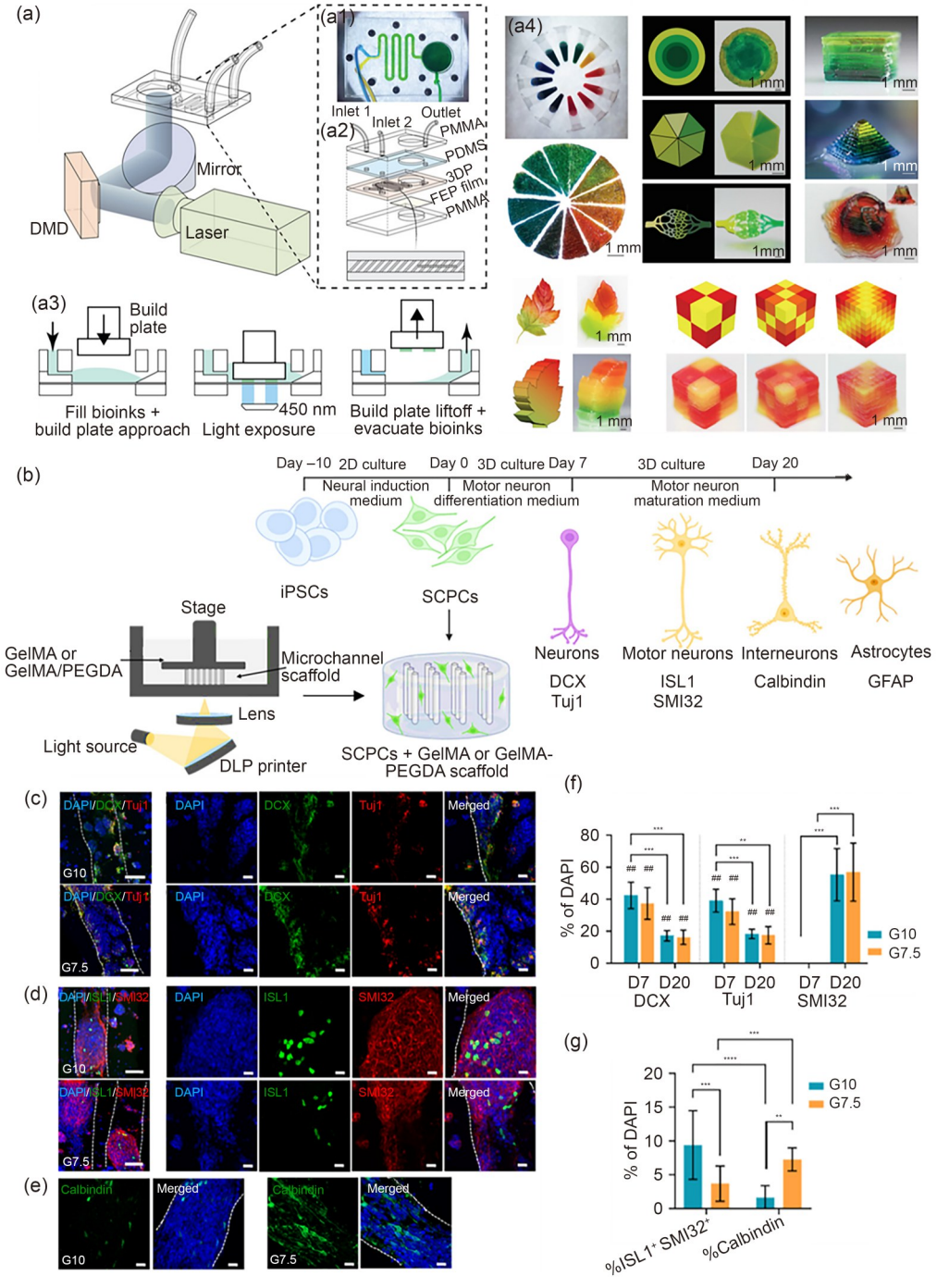

Fig. 5 Vat photopolymerization-based bioprinting. (a) Gradient DLP bioprinter integrating a DLP system with a microfluidic mixing chip: (a1) photograph of the chip showing blue and yellow inputs mixed into green via a chaotic mixing microchannel and bio-ink vat; (a2) assembly of the chip with two inlets, one outlet, and a slanted-rib mixing channel; (a3) gradient DLP printing workflow, involving continuous bio-ink mixing, photo-crosslinking, and postprinting removal of residual ink for each gradient; (a4) representative 2D and 3D structures produced using composable-gradient DLP printing. Reproduced from [74], with permission from Wiley-VCH GmbH. (b) Single-layer DLP printing of GelMA-based microchannel scaffolds seeded with human induced pluripotent stem cell (iPSC)-derived SCPCs. SCPCs were induced in 2D culture (Days −10 to 0), encapsulated on Day 0 in GelMA or GelMA/PEGDA, and printed into 3D scaffolds under 405 nm light (25 mW/cm^2). After washing, the scaffolds were cultured in motor neuron differentiation medium until Day 7 and in maturation medium until Day 20 to generate motor neurons, interneurons, and astrocytes. Representative confocal images of DCX$^+$ and Tuj1$^+$ early neurons (c), ISL1$^+$ and SMI32$^+$ motor neurons (d), and Calbindin$^+$ interneurons (e) in G10 and G7.5 scaffolds after 20 d. For (c, d), images were acquired at 20× (the first column) and 40× (the remaining columns) magnification. White dashed lines denote the microchannel walls. Scale bars: 50 μm (n=3). (f) Quantitative analysis of DCX, Tuj1, and SMI32 expression in G10 and G7.5 after 7 and 20 d. (g) Quantitative analysis of ISL1$^+$, SMI32$^+$, and Calbindin expression in G10 and G7.5. Reproduced from [75], with permission from the American Chemical Society

Encouragingly, recent AM studies have demonstrated that carefully optimized BJP parameters yield highly interconnected porous Mg-based scaffolds with bone-mimicking properties. Mg–Zn–Zr scaffolds with 13% porosity, median pore sizes of ~12.7 μm, and interconnectivity exceeding 95% have been fabricated, exhibiting a tensile strength of ~130 MPa, an elastic modulus of ~21.5 GPa, and a compressive strength of ~349 MPa, values comparable to cortical bone [77]. In vitro assessments have indicated favorable biological responses, with BJP Mg–Zn–Zr alloys demonstrating Level 0 cytotoxicity and enhanced MC3T3-E1 cell viability, attachment, and proliferation relative to cast counterparts (Fig. 6a). Nevertheless, translating these encouraging results into reliable in vivo performance remains uncertain, as degradation-induced mechanical property loss under physiological conditions has yet to be fully quantified. Long-term in vivo studies correlating pore architecture, corrosion behavior, and load-bearing capacity, therefore, remain a critical research gap.

To address challenges related to contamination and densification during AM, alternative processing strategies are being explored. Binderless 3D printing combined with liquid-phase sintering enables the production of Mg scaffolds without organic binders, reducing impurity incorporation while achieving bone-mimicking porosity and mechanical properties [78]. Despite these advances, corrosion remains a key limitation: electrochemical testing and hydrogen evolution measurements have shown that porous Mg–Zn–Zr scaffolds degrade significantly faster than dense counterparts due to

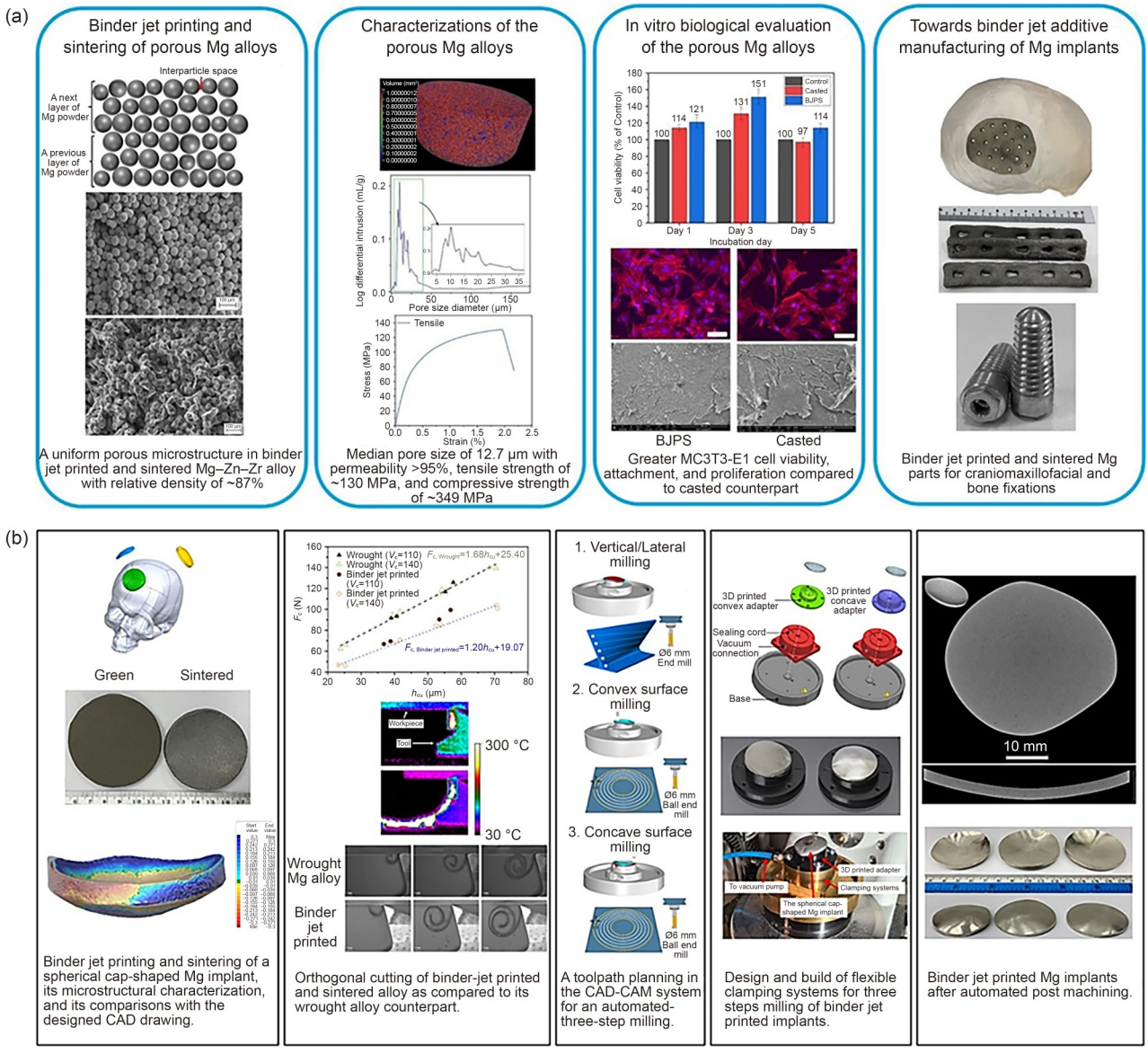

Fig. 6 Additive manufacturing of magnesium alloys. (a) Achieving the biomimetic porosity and strength of bone in magnesium scaffolds through binder jet additive manufacturing. Reproduced from [77], with permission from Elsevier B.V. (b) An end-to-end digital hybrid manufacturing process workflow was established to produce personalized Mg implants. Reproduced from [84], with permission from Chongqing University

localized corrosion along pore walls [79]. Surface engineering strategies, including hydroxyapatite impregnation and thin polymer coatings, retard corrosion, but their long-term durability and effectiveness throughout the entire in vivo degradation period remain areas of investigation.

Additional improvements in print quality and mechanical performance have been achieved through powder engineering and microstructural control. Adding 0.2% calcium nanoparticles (mass fraction) to Mg−Zn−Zr powders enhances sintering kinetics, increasing densification rates by ~25%, leading to significant improvements in tensile strength (~30%), compressive strength (~15%), elastic modulus (~18%), and elongation (~185%) [80]. Meanwhile, microwave (MW) sintering has emerged as an efficient consolidation route, providing rapid densification with processing time reduced by a factor of three compared with conventional sintering, while preserving interconnected porosity and bone-like mechanical responses [81]. When integrated with binderless AM, MW sintering facilitates the fabrication of chemically pure Mg components with minimal contamination [82]. At a mechanistic level, capillarity-driven interparticle bridging is a key consolidation pathway during ambient-temperature printing: native MgO surface films convert into in situ solid bridges and subsequently decompose cleanly during sintering, offering a binder-free AM approach for processing Mg and other oxidation-prone metals [82, 83].

From a manufacturing perspective, end-to-end digital manufacturing workflows integrating AM with automated dry postmachining have enabled the creation of near-net-shape Mg implants with high dimensional fidelity, reproducibility, and surface roughness <1.3 μm after precision milling [84]. Such digital workflows reveal a scalable, reproducible route to producing patient-specific biodegradable implants with high geometric fidelity (Fig. 6b). Nevertheless, dimensional fidelity alone is insufficient to guarantee clinical success, as in vivo degradation may alter the implant geometry and surface conditions over time, potentially compromising functional performance.

Overall, advances in alloy design, powder engineering, consolidation mechanisms, corrosion mitigation strategies, and digitally integrated postprocessing have significantly expanded the feasibility of using Mg alloys for biomedical AM. Together, these developments establish a robust technological foundation for the next generation of resorbable metallic implants tailored for personalized and regenerative medicine.

3.3.2 Titanium alloys

Titanium and its alloys remain the gold standard for permanent orthopedic and dental implants due to their excellent biocompatibility, high strength-to-weight ratio, corrosion resistance, and compatibility with complex geometries produced by AM. However, the commonly used Ti–6Al–4V poses long-term cytotoxicity risks associated with aluminum and vanadium ion release, motivating the development of safer β-phase Ti alloys such as titanium–tantalum (Ti–Ta) [85].

Laser powder bed fusion (LPBF) has played a central role in advancing Ti–Ta alloys by enabling in situ alloying, which allows precise composition and microstructure tuning during fabrication. Using controlled laser processing strategies, Ti–Ta alloys have been manufactured with significantly higher tensile strength and markedly lower Young's modulus than commercially pure Ti or Ti–6Al–4V [85]. This synergistic mechanical profile is ideal for orthopedic applications, where reducing stiffness mismatch mitigates the stress shielding effect while avoiding cytotoxic alloying elements.

Further optimization has expanded microstructural control in Ti–50Ta alloys. By systematically mapping process–structure–property relationships, including laser power, scanning speed, and layer thickness, comprehensive databases have been established that capture the influence of tantalum content on mechanical behavior, corrosion resistance, and wear performance (Fig. 7a) [86]. These maps support reproducible fabrication and facilitate patient-specific material customization.

At the microstructural level, achieving uniform compositional distribution remains a key challenge for β-phase titanium alloys. This has been addressed by intentionally promoting the formation of orthorhombic α″ martensite during rapid solidification (Fig. 7b) [87]. Incorporating this phase enhances lattice distortion and strain adaptability, offering Ti–30Ta alloys with improved ultimate tensile strength while maintaining a consistently low Young's modulus, an uncommon but highly desirable property combination for loading-bearing implants. In vitro assessments further confirmed excellent biocompatibility and osteogenic support.

Alongside alloy chemistry, implant geometry and architectural design play critical roles in determining mechanical performance. Investigations into LPBF-fabricated lattice structures revealed strong correlations between strut size and structural strength [88]. A regression analysis method provides quantitative predictions of these relationships, allowing mechanical behavior to be tuned through precise adjustment of process parameters such as laser power and scanning speed. A study demonstrated that optimized lattice designs can achieve high geometric fidelity and tailored mechanical properties. Complementary finite element analysis provides accurate elastic modulus predictions across porosities ranging from 50% to 90%, with excellent agreement with the Gibson–Ashby model (Fig. 7c) [89]. This combined experimental–computational framework accelerates lattice optimization and enhances confidence in the load-bearing performance of implants.

Advances in the AM of Mg and Ti alloys demonstrate how material innovation, microstructural engineering, consolidation

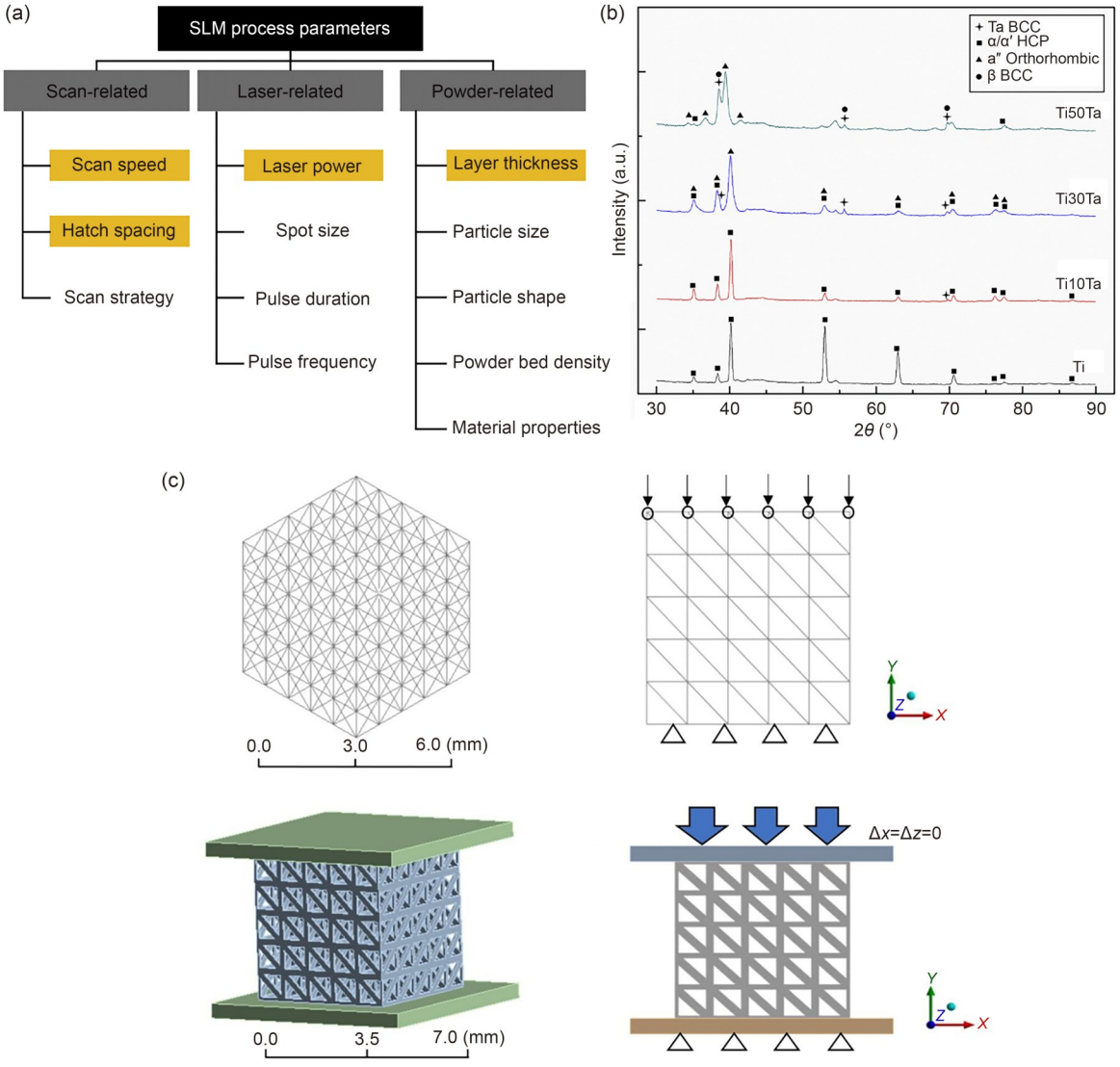

Fig. 7 Additive manufacturing of titanium alloys. (a) Schematic diagram of the in situ alloying process control for the Ti–50Ta alloy. Reproduced from [86], with permission from Elsevier Ltd. (b) X-ray diffraction (XRD) results of the orthorhombic martensitic structure of Ti–30Ta alloy. Reproduced from [87], with permission from Elsevier Ltd. (c) Schematic diagram of stress on the lattice structure under finite element analysis. Reproduced from [89], licensed under CC BY 4.0

mechanisms, and computational design converge to produce high-performance metallic implants. Whereas Mg alloys offer pathways to biodegradable, bone-mimetic scaffolds, Ti–Ta systems provide durable and biocompatible solutions for long-term implantation. These developments complement soft-material fabrication technologies like electrospinning and 3D bioprinting, forming a multimaterial foundation for future biomanufacturing.

4 Emerging applications

As biomanufacturing continues to develop, a diverse set of emerging applications (beyond those traditionally associated with biomedical engineering) is reshaping the biomanufacturing landscape. These innovations reflect the expanding reach of engineered biological systems into therapeutics, food production, and bioelectronics. In this section, we highlight five rapidly advancing domains: (1) ML-assisted AM, (2) food biomanufacturing, (3) regenerative cell therapy, (4) microneedle systems for therapeutic applications, and (5) bioelectronics to illustrate how converging advances in materials science, digital design, and biological engineering are defining the next generation of biomanufacturing capabilities.

4.1 Machine learning-assisted additive manufacturing

ML has emerged as a powerful enabler in AM, offering predictive insights to complement traditional process optimization

and materials engineering [90–92]. As printing systems become increasingly complex, ML offers the analytical capacity to model nonlinear behaviors, reduce trial-and-error, and provide real-time quality assurance. This subsection highlights how ML is being deployed across different parts of biomanufacturing workflows, progressing from soft-material bioprinting to alloy design and microstructural interpretation, and then to defect detection and forecasting in metal AM.

In bioprinting, a key challenge is the stochastic nature of cell distribution during droplet formation, which is difficult to capture solely through analytical modeling. To address this, ML has been used to predict cell numbers in inkjet-ejected droplets by analyzing droplet velocity deceleration across two positions [93]. High-speed optical imaging (120,000 frames/s) captured trajectories of PVP-based bio-ink droplets containing 1–3 million primary human dermal fibroblasts per milliliter, generating 156 annotated trajectories. Five supervised learning models were trained on velocity-derived features: the random forest model achieved the highest balanced accuracy (~82%) for classifying whether the droplets contained cells, whereas extra trees provided the most accurate multi-droplet cell count estimates, reducing the prediction error to 12% (vs. the 23% baseline). These findings highlight the potential of ML-enabled droplet-level monitoring systems for real-time regulation of cell density in jetting-based bioprinting.

In addition to soft biomaterials, ML has become increasingly important for accelerating alloy discovery and predicting mechanical performance in AM-produced metals, where complex interactions between composition, thermal history, and phase evolution present significant optimization challenges. A recent metallurgy-guided ML framework demonstrated how the calculation of phase diagrams and thermodynamic simulations can be coupled with ML to design Fe–Cr–Co–C martensitic stainless steel tailored for AM (Fig. 8a) [94]. A design-of-experiments sweep across Cr (10.0%–14.5%, mass fraction), Co (0%–5.0%, mass fraction), and C (0.15%–0.40%, mass fraction) produced simulated descriptors including the solidification freezing range (SFR), hot cracking susceptibility (HCS), growth restriction factor (GRF), and precipitation speed of carbides (PSC). Despite a moderate dataset size, ML models achieved high predictive accuracy: the random forest model performed best for HCS, GRF, and SFR (R^2=0.999–1.000), whereas k-nearest neighbors (KNN) predicted PSC with R^2=0.996. Multi-objective optimization using non-dominated sorting genetic algorithm III (NSGA-III) generated alloy candidates that were experimentally validated, exhibiting yield strengths of 1062–1769 MPa and uniform elongations of 2.1%–11.7%. A parallel study on Ti–Ta alloy development introduced the concept of "in situ alloying degree," a quantitative measure of compositional homogeneity during AM (Fig. 8b) [95]. By integrating this metric with a comprehensive experimental dataset, ML models identified nonlinear correlations between processing parameters and microstructural outcomes, accelerating alloy optimization and reducing the materials and time cost associated with conventional trial-and-error strategies.

Complementing alloy discovery, ML has also been applied to understand the microstructural influences on mechanical properties in AM-fabricated Ti–6Al–4V. A fuzzified ML framework based on an adaptive neuro-fuzzy inference system (ANFIS) was trained on 120 LPBF samples with densities of 96.1%–98.8%, fabricated across laser powers of 120–340 W [96]. The measured Young's modulus served as the ground truth, derived from ultrasonic longitudinal and shear velocity measurements. ANFIS achieved a validation error of only 0.66 GPa, far outperforming the Gibson–Ashby model for low-porosity samples. This approach further introduced a deviation factor (δ) that quantitatively captures microstructural effects, such as pore topology and phase distribution, that influenced the modulus. A secondary ANFIS model predicted δ with a test error of 3.7189 (95% confidence interval: −1.54 to 1.48), demonstrating its reproducibility. Together, these findings highlight how ML can elucidate structure–property relationships that are otherwise obscured in complex AM microstructures, strengthening the predictive basis for process and material optimization.

As AM advances toward production-scale deployment, ensuring build integrity via real-time monitoring has become a priority. Spatiotemporal deep learning is particularly effective in capturing the melt-pool dynamics during LPBF, where defects often arise abruptly. A convolutional recurrent neural network (C-RNN) was developed to detect overhanging scan vectors—predictive indicators of surface-quality degradation—using open-access melt-pool videos (10,000 Hz coaxial imaging) [97]. The model was trained on the X4 build and validated on the independent X16 build. Despite the extreme class imbalance (~0.65% positive frames), the optimized C-RNN achieved >99% overall accuracy. On a representative layer, it attained a precision of 0.89 and a recall of 0.72 with a false-positive rate as low as 0.002. Importantly, inference for an entire layer required only 107 s, approaching near-real-time implementation. These results show that incorporating temporal information greatly enhances defect detection beyond spatial-only approaches, offering a practical pathway for automated in situ quality control.

Although deep learning enables the detection of defects that have already emerged, recent advances in time-series foundation models extend this capability to predict defects before they form, supporting proactive, rather than reactive, process control. Their performance was evaluated on two real-world AM monitoring datasets [98]. The first dataset comprised 24,800 labeled layers from Ti–6Al–4V LPBF builds, each containing 60 eddy-current testing (ECT) features, with the porosity determined via metallography. The second dataset included 1557 pyrometer images converted into directional temperature profiles and labeled via X-ray

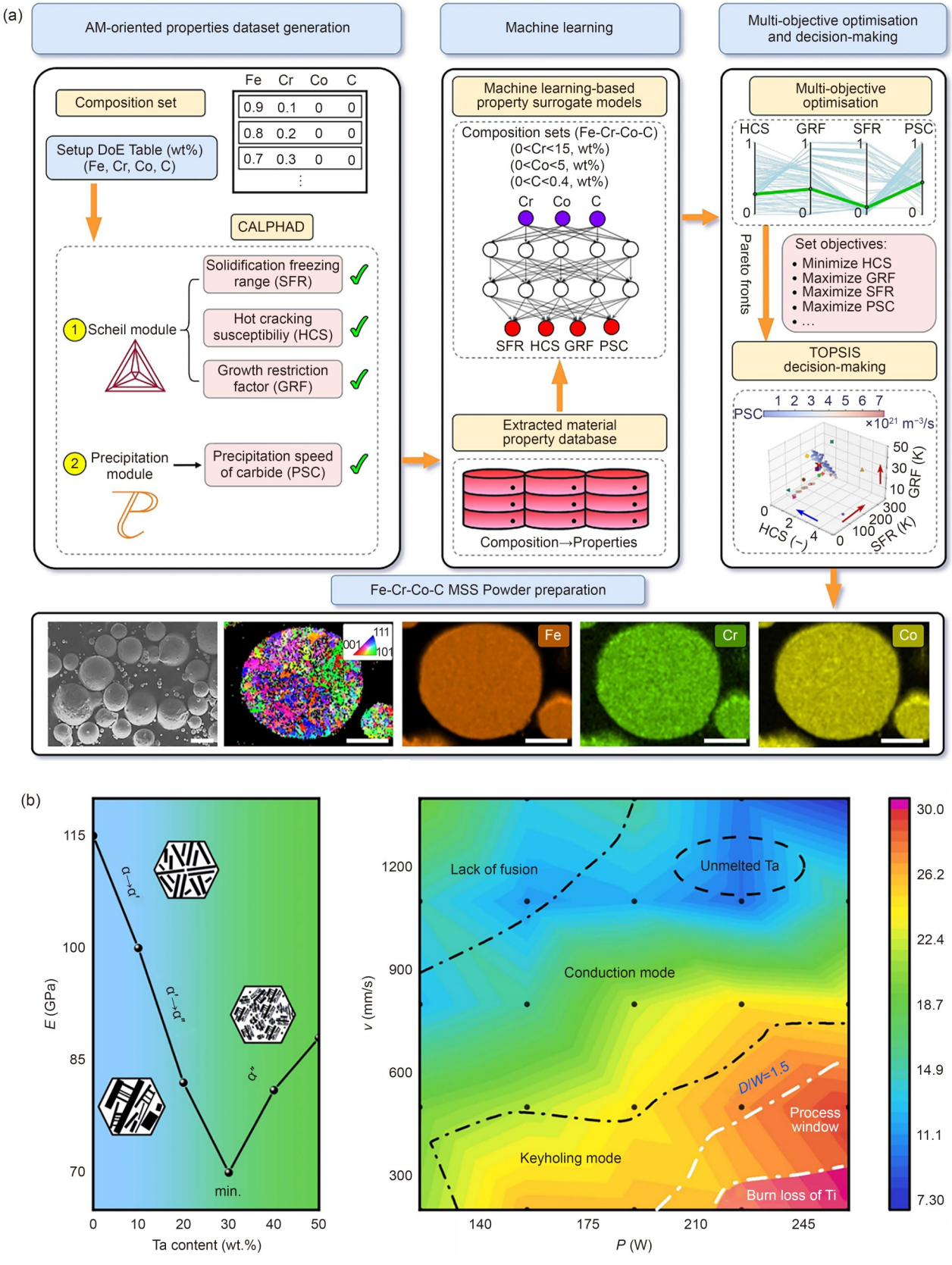

Fig. 8 ML-assisted AM. (a) Schematic of the AM metallurgy-guided ML framework used for martensitic steel design. Reproduced from [94], with permission from Elsevier Ltd. (b) Ti–30Ta in situ alloying process map integrating ML predictions with in situ alloying degree measurements. Reproduced from [95], with permission from Elsevier B.V.

computed tomography (XCT). Three foundation models (GPT4TS, TimeLLM, and UniTS) were minimally fine-tuned on patch-embedded time-series inputs for up to 20 epochs. For ECT-based porosity forecasting, GPT4TS achieved the lowest mean absolute error (MAE, 0.1022) using only four past layers—outperforming LSTM baselines requiring far longer sequences. For pyrometer-based defect detection, GPT4TS achieved an F1-score of 97.88%, surpassing benchmarks such as PyroNet (90.89%) and Res-RCNN (94.70%). These findings show that foundation models offer generalizable, data-efficient predictors that capture subtle temporal dependencies and forecast porosity before it manifests, enabling increasingly autonomous AM systems.

These studies highlight the expanding role of ML as an essential component of modern biomanufacturing. From predicting cell deposition in bioprinting to guiding alloy design, interpreting microstructural effects, and enabling real-time defect detection and forecasting, ML provides quantitative insights previously inaccessible using empirical or physics-based approaches alone. Looking forward, ML is poised to become deeply embedded within closed-loop biomanufacturing pipelines, optimizing biomaterials, processes, and quality control simultaneously. Integrating ML across soft- and hard-material biofabrication establishes a foundation for predictive, reliable, and intelligent biomanufacturing ecosystems that can support next-generation biomedical applications.

4.2 Food biomanufacturing

As global demand for sustainable and ethical protein sources increases, food biomanufacturing has emerged as an alternative approach to producing structured, nutritious, and sustainable food products. This rapidly expanding field encompasses a continuum of technologies ranging from cell-based cultivated meat (CM) to acellular protein scaffolds. Whereas CM depends on living cells to generate edible tissues, plant-derived and hybrid structuring technologies offer complementary pathways to fabricate food architectures with customizable textures, sensory qualities, and nutritional profiles. Together, these approaches form an integrated biomanufacturing landscape that can be selectively combined to address diverse functional, sensory, and sustainability goals.

A major focus in CM production is developing edible scaffolds that support muscle cell attachment, proliferation, and differentiation. Electrohydrodynamic printing has been applied to produce highly ordered, ultrafine fibrous scaffolds suited for CM applications (Fig. 9a). Composite inks formulated from zein blended with higher-molecular-weight cereal prolamins such as hordein (barley) or secalin (rye) provide the rheological properties required for stable jetting and fiber solidification [99]. These plant-derived inks (>90% purity) facilitated the fabrication of tessellated scaffolds with 400-μm pores and mechanical stiffness ~4× that of PCL. When seeded with mouse C2C12 myoblasts or porcine skeletal satellite cells (PSCs), the scaffolds supported a 10–30-fold increase in cell number over 11 d, with robust alignment along the ~20 μm fibers and expression of key myogenic markers such as desmin, myogenin (MYOG), and myosin heavy chain. A whole-cut CM prototype produced by culturing PSCs on zein/secalin scaffolds provided substantial tissue formation, shrinking by 28.6% and increasing in mass by 59.3%. Although prolamins have limited essential amino acid content, their edibility, low cost, and degradability make them attractive for integration into hybrid CM products.

To further streamline CM bioprocessing, a complementary plant-derived biomanufacturing strategy combines edible scaffolds with serum-reducing nutrient systems [100]. Plant protein hydrolysates derived from enzymatically hydrolyzed soy and wheat proteins were incorporated into the culture media, reducing fetal bovine serum requirements from 10% to 3%–4% while sustaining PSC proliferation and stemness (*PAX7* expression). Textured plant protein scaffolds derived from peanut protein provided a highly porous matrix that promoted myotube alignment and cell infiltration. The resulting cultivated pork prototype had an enhanced protein content (~16% for the CM prototype vs. 12% for the scaffold alone), improved hardness and chewiness, and released a desirable meat-like aroma upon cooking, demonstrating that plant-derived scaffolds and bioactive media additives can together lower costs and enhance CM quality.

Another approach uses decellularized plant scaffolds, exploiting naturally occurring plant vasculature to guide muscle cell organization [101]. White asparagus stems were decellularized using SDS and Triton-X, followed by calcium chloride and freeze-drying, producing cellulose-, hemicellulose-, and pectin-rich scaffolds with intact vascular bundles. These structures supported the proliferation and differentiation of C2C12 myoblasts and porcine adipose-derived mesenchymal stem cells, enabling the formation of cocultured muscle–fat constructs with aligned myotubes and lipid-rich adipocytes. The uncooked CM prototypes exhibited textural properties comparable to pork loin and turned brown upon pan-frying due to Maillard reactions.

Beyond cell-based systems, food biomanufacturing also encompasses acellular approaches to producing plant- or marine-protein food analogs with biomimetic textures. One example involves salmon fillet analog formation using extrusion-based 3D food printing coupled with enzymatic texturization [102]. In that study, pea protein emulsions, optimized via high-pressure homogenization and maintained at ⩾30% oil content for printability, were printed to replicate salmon's myosepta architecture. Postprinting treatment with transglutaminase enhanced structural cohesion and mechanical strength. The resulting plant-derived fillet analog reproduced the characteristic alternating fat–muscle morphology of salmon, offering a

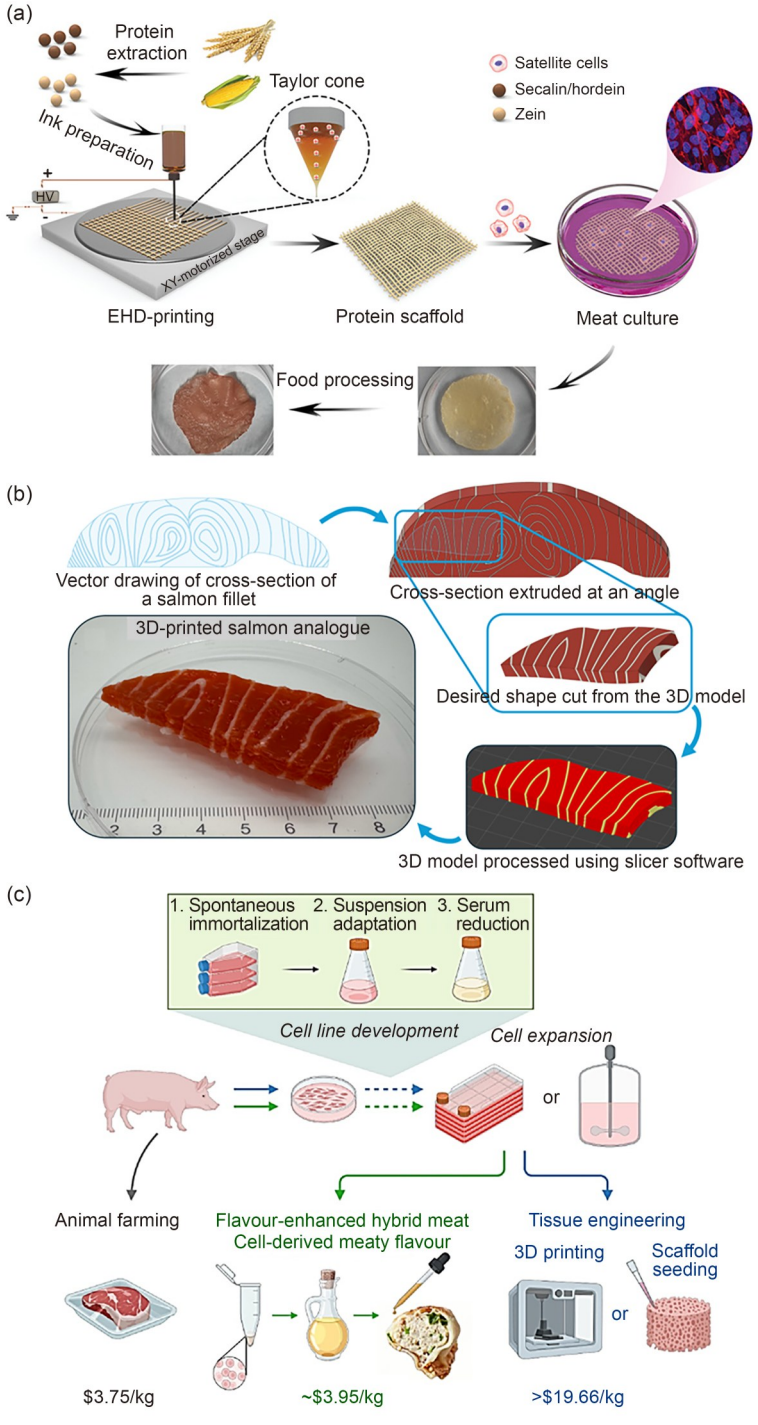

Fig. 9 Food biomanufacturing spanning cell-based CM to acellular protein scaffolds. (a) Schematic illustration of the CM model fabricated using prolamin-based edible scaffolds produced via electrohydrodynamic printing. Composite plant–protein inks enable the generation of ultrafine fibrous architectures that support muscle cell proliferation and differentiation. Reproduced from [99], with permission from Wiley-VCH GmbH. (b) Workflow for generating 3D-printed salmon analogs in the form of sashimi slices. A vector illustration of a salmon fillet cross-section is first created and extruded at a defined angle to obtain a 3D fillet segment. A representative sashimi slice is then extracted from this segment and processed with commercial slicing software to generate the corresponding G-code. The G-code directs the printer to deposit food ink, with myomeres (muscle structures) indicated in red and myosepta (connective tissues) in white, yielding a biomimetic salmon analog. Reproduced from [103], under exclusive licence to Springer Science Business Media, LLC, part of Springer Nature. (c) Spontaneously immortalized, suspension-adapted porcine cells are used as biocatalysts to produce authentic meat aroma precursors. Cells expanded in 1% serum are lysed to release proteins and lipids that undergo Maillard and lipid thermal degradation reactions when heated in oil at 140 °C, generating a volatile profile closely resembling cooked pork. Incorporation of only 1.2% (mass ratio) of this aroma extract into plant-derived matrices yields hybrid pork analogs with a sensory similarity score of 78.5%, reducing production costs by ~80% relative to conventional CM. Reproduced from [104], licensed under CC-BY-NC

nutritional profile influenced by the protein-rich (5.5% protein) and lipid-rich emulsion layers. This approach highlights how acellular structuring can yield visually and texturally convincing seafood alternatives without relying on animal cell cultures.

In another study, salmon sashimi analogs were manufactured using extrusion-based 3D printing of hydrogels composed of fish gelatin and gellan gum (Fig. 9b) [103]. Fish gelatin is abundant and inexpensive, with good digestibility, whereas gellan gum enhances printability and thermal stability. Rheological characterization revealed robust conformity to the Ostwald–de Waele model (R^2>0.95) and rapid thixotropic recovery, enabling high-fidelity printing. After optimization, a 10:1 gelatin:gellan gum formulation achieved the best balance of hardness, cohesiveness, and chewiness. These material-engineering strategies highlight how acellular food inks can be customized to produce realistic, protein-rich analogs without the technical constraints of cell culture.

A distinct yet complementary sensory biomanufacturing strategy involves engineering for flavor rather than structure. Recent work illustrates that spontaneously immortalized porcine cells can be used as biocatalysts to produce authentic meat aromas (Fig. 9c) [104]. Suspension-adapted porcine myoblasts and fibroblasts were expanded to high cell densities (~$(21-29)\times10^6$ cells/mL) under 1% serum conditions and lysed to release proteins and lipids to serve as precursors for Maillard and lipid thermal degradation reactions. Heating these precursors in oil at 140 °C yielded a volatile profile like a cooked meat aroma. Notably, incorporating only 1.2% (mass ratio) aroma extract into plant-derived matrices yielded hybrid pork analogs with a sensory similarity score of 78.5%. This approach bypasses tissue production complexities and reduces cell-related costs by ~80% compared to conventional CM, offering a scalable method to enhance flavor realism in alternative proteins.

Finally, 3D food printing offers a platform for producing personalized, texture-modified foods for vulnerable populations, like individuals with dysphagia. Recent studies have shown that fresh vegetables (e.g., garden pea, carrot, and bok choy) [105] or vegetable food waste streams (e.g., spinach stems and kale stalks) [106] can be transformed into printable food inks using hydrocolloids such as agar, gelatin, xanthan gum, kappa-carrageenan, and locust bean gum. These formulations exhibit shear-thinning rheology and structural stability compatible with extrusion printing while meeting International Dysphagia Diet Standardization Initiative safety criteria for dysphagia diets. Importantly, using fresh or waste vegetables preserves nutritional content, improves visual appeal, and reduces food waste. By integrating rheology control with AM, 3D food printing allows the scalable production of customized meals that support safety and patient acceptance in clinical nutrition.

Together, these examples illustrate the breadth of modern food biomanufacturing, spanning engineered cell-based tissues, plant-derived scaffolds, acellular seafood analogs, flavor-enhanced hybrid foods, and personalized clinical nutrition solutions. By integrating biomaterials science, cell biology, and AM, these technologies offer complementary pathways toward sustainable, nutritious, and customized food products. Nevertheless, significant challenges remain, particularly regarding consumer acceptance of cultivated and texture-modified foods and consumer perception related to safety, naturalness, and long-term health implications [107]. Addressing these challenges via public engagement, transparent regulation, and continued technological refinement is essential for the widespread adoption of food biomanufacturing.

4.3 Regenerative cell therapy

Regenerative cell therapy is increasingly recognized as a core pillar of future biomanufacturing, offering the potential to restore or replace dysfunctional tissues across many chronic diseases. Advances in stem cell biology, human disease modeling, biomaterials, and biofabrication have collectively accelerated the development of scalable, regulatory-aligned cell-based therapies. This subsection highlights two major domains (diabetes and ocular regeneration) where biological systems and engineering innovations are converging within the biomanufacturing landscape.

Glucose dysregulation arising from pancreatic β-cell dysfunction remains a central contributor to the global diabetes burden. Donor human islets, human pancreatic β-cell lines (e.g., EndoC-βH1) [108], and human pluripotent stem cell (hPSC)-derived islet-like cell availability [109, 110] have dramatically enhanced the resolution at which human β-cell failure has been studied over the past two decades. These platforms have permitted the detailed interrogation of monogenic diabetes, including maturity-onset diabetes of the young (MODY) subtypes [111–116] and East Asian type 2 diabetes associated with *PAX4* variants [117], elucidating how specific mutations impair β-cell function, survival, and insulin secretion. These insights have expanded our understanding of diabetes pathogenesis and accelerated therapeutic target discovery.

In addition to disease modeling, human pancreatic cell models are being utilized for drug studies and therapeutic development. hPSC-derived pancreatic cells have been used to examine the effects of metformin on early human development [118, 119] and to investigate how the anti-diabetic drug imeglimin enhances β-cell health and glycemic control in type 2 diabetes [120]. Ongoing efforts are elucidating the genetic regulators of insulin secretion using these systems to uncover molecular pathways with therapeutic potential [121]. Critically, hPSC-derived pancreatic islet-like cells serve as a foundation for β-cell replacement therapy in diabetes [122].

These cells can be integrated with biomaterial scaffolds, vascularization strategies, and various encapsulation platforms to enhance cell survival and immunoprotection [123]. Advances in biofabrication, including 3D bioprinting and high-throughput cell manufacturing, further support future scalability for transplantation and drug screening [124].

Cell therapy and biomaterial engineering also play a central role in corneal regeneration, addressing critical shortages in donor tissues and limitations of traditional grafting techniques. A suite of biofabrication strategies has emerged to restore epithelial, stromal, and endothelial function in the diseased cornea. Biofabricated epithelial grafts generated with accelerated, ice-cold urea-based de-epithelialization of human amniotic membranes preserve native basement membrane cues and enable efficient cell seeding [125]. Autologous conjunctival epithelial cells cultured on these scaffolds have achieved complete ocular surface epithelialization in clinical application [126].

For advanced ocular surface failure, where biological grafts are contraindicated, engineered spark-plasma-sintered titania–graphene oxide composites exhibit high mechanical strength, corrosion resistance, and long-term stability. These properties have positioned this material as a synthetic keratoprosthesis skirt to replace tooth-derived substrates used in osteo–odonto keratoprosthesis [127]. Keratocyte-based therapies have shown restoration of stromal transparency and ultrastructure after microinjection in preclinical models (Fig. 10a) [128, 129]. Complementary strategies repurpose the stromal lenticules obtained from refractive surgeries, with demonstrated safety and efficacy in primate and keratoconus patient models [130–132]. Establishing a lenticule bank supports standardized processing and storage, enabling future applications such as presbyopic inlays [133, 134]. Electron-beam sterilization further enables room-temperature storage of corneal tissues for up to two years [135], whereas decellularized lenticules have been used as drug depots delivering bioactive factors like nerve growth factor to promote nerve regeneration [136].

Treatment of endothelial dysfunction has advanced with two complementary approaches: (1) simple noncultured endothelial cell (SNEC) injection, which isolates viable corneal endothelial cells (CECs) from donor Descemet's membranes through mild dissociation [137]; (2) tissue-engineered endothelial keratoplasty (TE-EK) or via corneal endothelial cell injection (CE-CI), relying on dual-media expanded CECs [138, 139]. Both strategies have demonstrated corneal clarity and endothelial function restoration in rabbit models (Fig. 10b). A first-in-human TE-EK clinical trial has been initiated (ClinicalTrials.gov NCT04319848). Additionally, codeveloping Health Science Authority (HSA)-aligned SNEC and CEC injections broaden delivery options, alongside ongoing scaffold material, shipping logistics, and manufacturing workflow optimization.

For diabetes and ocular diseases, a unifying theme is integrating stem cell biology, biomaterials engineering, and biofabrication technologies to create functional cell-based therapeutics. These developments reflect a broader shift in biomanufacturing toward scalable, automated, and quality-controlled platforms capable of producing complex biological products. Continued advances in differentiation protocols, genetic engineering, biomaterial design, and Good Manufacturing Practice (GMP)-aligned manufacturing will be important for the widespread clinical translation of cell therapies.

4.4 Microneedle systems for therapeutic applications

Microneedle (MN) systems have emerged as versatile, minimally invasive platforms for transdermal therapeutic delivery and biomarker extraction [140]. Their microscale architecture facilitates painless stratum corneum penetration, allowing localized delivery of payloads, including small molecules, nanoparticles, nucleic acids, living cells, engineered bacteria, and catalytic materials, while bypassing physiological skin barriers. Increasingly, MNs are being designed for bidirectional functionality, enabling both interstitial fluid (ISF) extraction for diagnostics and on-demand therapeutic agent release. This subsection highlights recent developments in MN technologies spanning scar and scarless wound healing, dermatological condition management, biosensing, and therapeutic delivery.

Dissolving hyaluronic acid (HA) MNs have been widely explored for nucleic acid delivery and scar modulation. One platform employed HA MNs fabricated with polydimethylsiloxane (PDMS) micro-molding into a 10×10 array of pyramidal needles (1000 μm height, 300 μm base side, and 5 μm tip radius) with 700-μm spacing and a 1-mm backing layer [141]. The MN tips were loaded with mesoporous silica-coated upconversion nanoparticles (UCNPs@mSiO_2) encapsulating molecular beacons or siRNA. Upon insertion, the HA matrix dissolved, releasing nanoparticles to deliver siRNA targeting the transforming growth factor-beta type I receptor (TGF-βR1) deep into the dermis, whereas the UCNP core enabled real-time luminescent tracking. The MNs achieved full penetration of mouse ear skin (~276 μm depth from an 800-μm tip) and sustained release of ~85% of loaded beacons over 72 h. A related HA-MN delivered tyramine-modified gelatin–siRNA nanoplex targeting secreted protein, acidic and rich in cysteine to reduce fibrosis [142], achieved gene knockdown in vitro and reduced scar formation in full-thickness excisional wounds in mice. Building on this work, a clinical study demonstrated that siRNA-loaded dissolving MN patches significantly reduced the postoperative scar volume compared to silicone sheets in contralateral controls, with high patient acceptability [143]. Together, these platforms reveal how dissolvable MNs can be engineered for

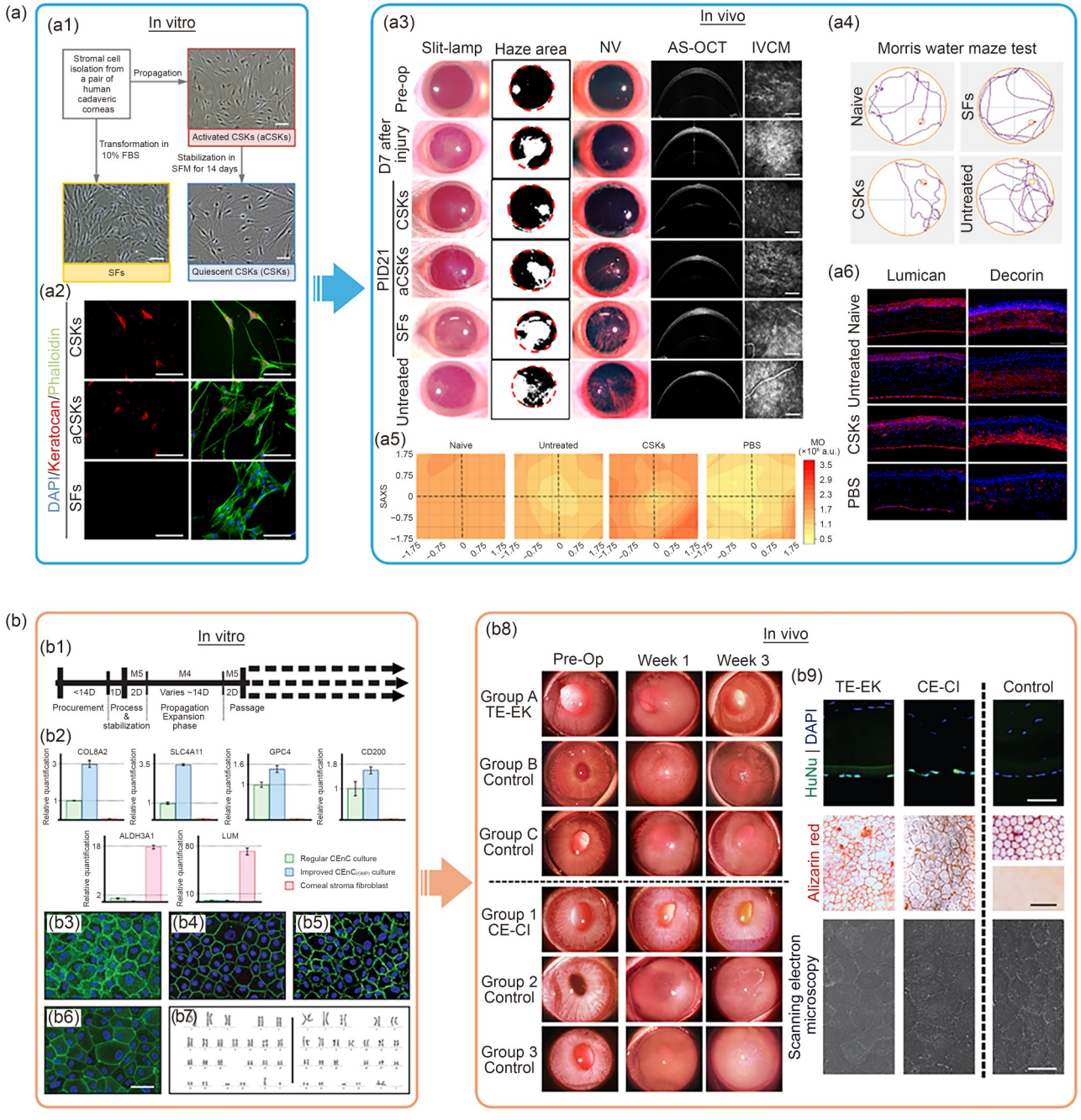

Fig. 10 Cell therapy approaches for corneal regeneration. (a) Stromal repair using corneal stromal keratocytes (CSKs): (a1) CSKs were expanded using a dual-media method, with serum-free medium promoting native marker recovery; (a2) keratocan expression was restored in CSKs but not in activated CSKs or fibroblasts; (a3, a4) in a rat stromal injury model, intrastromal CSK injection improved corneal transparency and visual function by Day 21 compared with untreated and fibroblast controls; (a5, a6) short-angle X-ray scattering confirmed native stromal ultrastructure restoration, accompanied by the recovery of keratan sulfate and dermatan sulfate proteoglycans (represented by lumican and decorin, respectively). Reproduced from [128, 129], licensed under CC BY 4.0. (b) Endothelial regeneration with CECs: (b1) schematic of the dual-media expansion approach; (b2–b6) expanded CECs maintained characteristic gene expression and protein markers (Na^+/K^+-ATPase, ZO-1, CD166, and PRDX-6) and exhibited a normal karyotype; (b7) representative chromosomal analysis revealed a normal karyotype in the cells at passage 3; (b8, b9) TE-EK and CE-CI restored corneal clarity in a rabbit bullous keratopathy model. The human origin of the transplanted cells was confirmed with HuNu staining, and imaging (Alizarin red/trypan blue and scanning electron microscopy (SEM)) showed characteristic polygonal morphology and surface microvilli. Reproduced from [138, 139], licensed under CC BY 4.0

precise, sustained intradermal gene modulation with translational potential.

Beyond delivery, MNs can serve as extractive immunomodulatory devices. Heparin-coated porous microneedles

(HPMNs) using a poly(lactic-co-glycolic acid) (PLGA)/$CaCO_3$ composite were molded and etched to create mechanically robust conical MNs with interconnected pores of >5 μm (Fig. 11a) [144]. Covalent grafting of a heparin/4-arm PEG-NH_2 (StarPEG) network onto pore surfaces generated dense sulfate groups able to bind positively charged chemokines, particularly monocyte chemotactic protein-1 (MCP-1), with high efficiency (81.6%±0.3%). This chemotactic sequestration recruited monocytes into MN pores, enabling them to be physically extracted upon patch removal. HPMNs reduced inflammatory signaling and monocyte burden in several preclinical models, accelerating diabetic wound healing (47.1% reduction in open wound area) in murine models, decreasing wound length in porcine models (27.2%), and reducing psoriatic inflammation when combined with immunosuppressants. These results illustrate a unique drug-free immunomodulation strategy based on localized chemokine and cell depletion.

Nanoparticle-based and dry powder-based MNs further expand the scope of transdermal bioactive delivery. Dry-powder dissolving MNs have been developed to co-deliver manganese dioxide (MnO_2) nanosheets and small-molecule anti-inflammatory agents (e. g., resveratrol) in solid-state formulations [145]. These MN patches typically comprise arrays of hundreds of polymeric cones, each several hundred micrometers long. Upon insertion into inflamed skin, the needles rapidly absorb ISF, dissolve, and then release MnO_2 and drug payloads in situ, enabling local oxidative stress and inflammatory pathway modulation. In preclinical skin-inflammation models, these dry-powder MNs achieved marked improvements in clinical scores and histological markers compared with topical administration, while minimizing systemic exposure.

Cryo-MNs extend the design space from molecular to cellular cargo. In one study, cryo-MNs were fabricated by stepwise cryogenic micro-molding of an optimized cryoprotective medium containing pre-suspended therapeutic cells into predesigned MN molds [146]. The resulting ice-based MNs had sufficient mechanical strength to pierce the skin, yet melted rapidly after insertion, releasing viable cells directly into defined skin layers (Fig. 11b). This platform maintained high post-thaw cell viability and enabled the local delivery of various cell types (e. g., immune or stem cells) in small animal models, supporting functional engraftment and disease-relevant therapeutic effects. A related cryo-MN system was adapted for ocular use, in which frozen MNs loaded with predatory bacteria were applied to the corneal surface to treat bacterial eye infections [147]. Upon application, the melting needles released bacteria locally onto the infected cornea, significantly reducing pathogen burden and improving clinical signs relative to conventional topical or injection-based therapies. Together, these studies demonstrate that MNs can be engineered to safely deliver a variety of bioactive agents from siRNA and nanoparticles to enzymes, small molecules, cells, and even bacteria with spatial precision and minimal invasiveness.

In addition to therapeutic delivery, MNs are increasingly used for minimally invasive biosensing and sampling. Osmosis-powered hydrogel MNs composed of methacrylated hyaluronic acid (MeHA) and maltose (Mal) have been engineered to rapidly extract microliter-scale volumes of ISF for downstream biomarker analysis (Fig. 11c) [148]. Fabricated by casting photo-crosslinkable MeHA-based precursors into molds, these swellable, mechanically robust MNs extracted (~7.90±0.92) μL of ISF from ex vivo porcine skin and (~3.82±0.60) μL from rat skin within 3 min for glucose quantification and other analyses. Complementing shallow ISF sampling, a transepidermal microprojection array (MPA) was developed to access deeper epidermal regions (≤200 μm) [149]. Created via high-resolution DLP printing with a Food and Drug Administration (FDA) Class IIa resin, the optimized cone-shaped array (22 mm×11 mm× 1.2 mm; 8×4 arrays) demonstrated high mechanical robustness (>1 N per projection) and superior microbial extraction efficiency. Overall, MPA offers a robust, depth-targeted complement to existing microbiome sampling tools (such as swabs and tape strips), enabling more spatially resolved investigation of skin microbial communities.

These studies exemplify the breadth and adaptability of MN systems as biofabrication-enabled platforms. By varying materials (HA, PLGA, MeHA, and cryoprotectants), structural formats (solid, porous, hydrogel, and cryogenic), and cargo types (siRNA, nanoparticles, catalytic agents, immune cells, and bacteria), MNs can be tailored for applications including scar modulation, immunomodulation, infection control, and real-time biomarker sampling. These advances illustrate how the rational integration of fabrication strategy, geometry, and cargo encapsulation allows MNs to function as precise, localized, and clinically relevant tools, positioning them as an important component of next-generation biomanufacturing and therapeutic delivery systems.

4.5 Bioelectronics

Bioelectronics has rapidly evolved into a field that merges materials science, electronics, and biology to create devices capable of sensing, stimulating, and interacting with living systems. Unlike conventional rigid electronics, bioelectronic devices are designed to match the softness, stretchability, and dynamic motion of biological tissues, enabling more intimate, stable interfaces. These systems support real-time physiological monitoring, closed-loop therapeutic feedback, and precision control of cellular behavior; functions that are increasingly essential for applications in tissue engineering, neural interfaces, wearable health monitoring, and implantable biomedical devices. As 3D tissue constructs and organ-on-chip

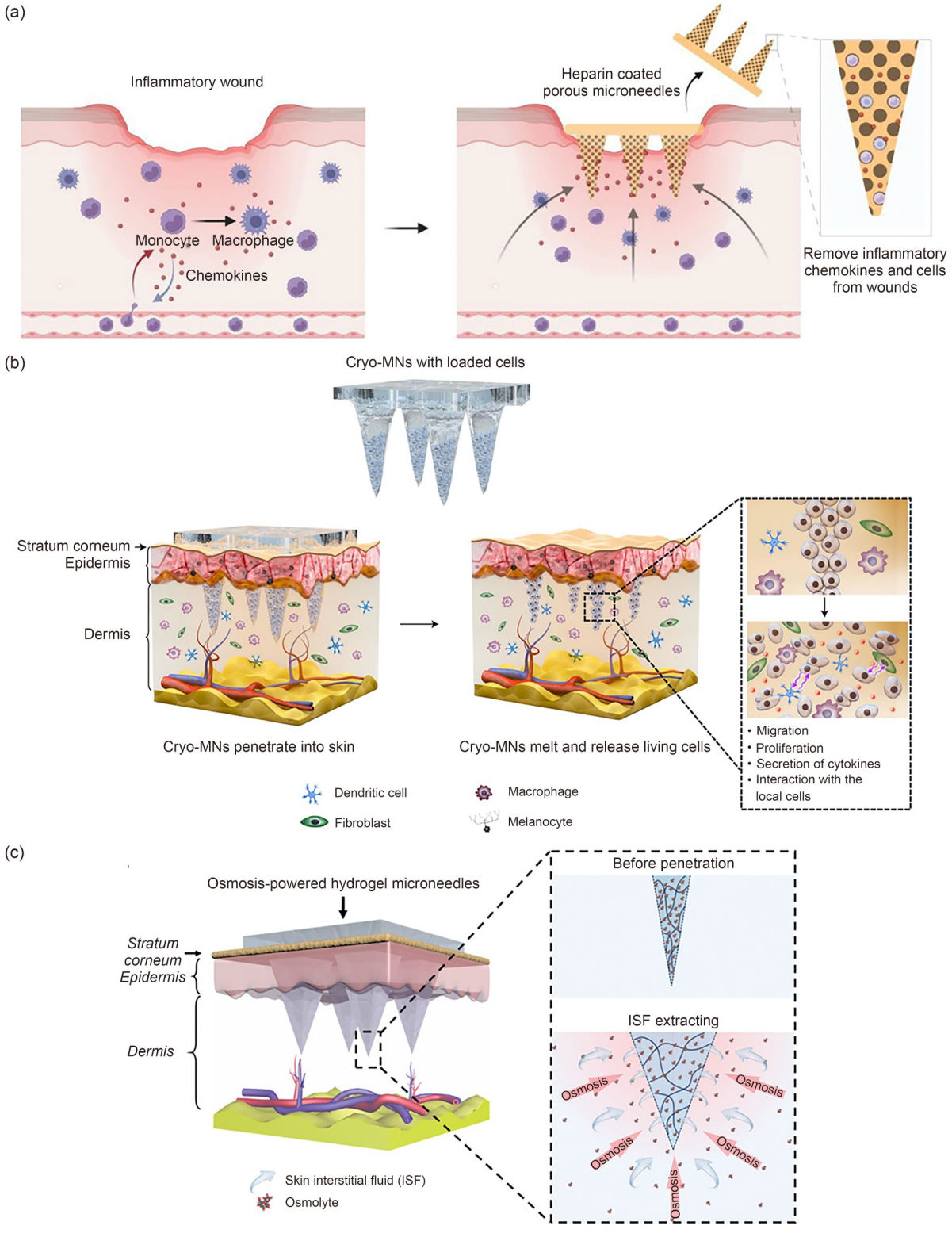

Fig. 11 Microneedle systems for therapeutic applications. (a) Schematic illustration showing how HPMNs bind and sequester chemokines, recruit inflammatory monocytes and macrophages, and are subsequently removed from the wound to facilitate tissue healing. Reproduced from [144], with permission from Wiley-VCH GmbH. (b) Transdermal delivery of cells with cryo-MNs. Cell-loaded cryo-MNs penetrate the epidermis, melt to release encapsulated cells, and enable subsequent cell migration, proliferation, cytokine secretion, and interaction with local skin cells. Reproduced from [146], under exclusive licence to Springer Nature Limited. (c) Osmosis-powered hydrogel MNs for interstitial fluid extraction. Schematic of fluid extraction driven by osmolyte-containing hydrogel MNs is shown. Reproduced from [148], with permission from WILEY-VCH Verlag GmbH & Co. KGaA, Weinheim

platforms become more physiologically sophisticated, the need for equally adaptive and biocompatible electronic interfaces has never been greater.

Traditional microfabrication strategies, such as photolithography and templating, have provided major advances in bioelectronics but are limited by high costs, rigid substrates, and complex cleanroom requirements. Printing-based approaches offer a compelling alternative: they enable rapid prototyping, geometric customization, the integration of diverse materials, and compatibility with soft and irregular substrates. However, with printed electronics, challenges remain, including resolution limits, ink rheology constraints, and difficulties in producing free-standing or 3D microstructures using conductive materials. Recent advances in AM have begun to directly address these limitations, providing pathways toward fully printed, conformal, and mechanically adaptive bioelectronic systems.

Among these innovations, aerosol jet printing (AJP) has emerged as a versatile maskless fabrication method for flexible multielectrode arrays (MEAs). AJP provides direct deposition of gold nanoparticle inks onto ultrathin polyimide substrates with microscale precision [150]. By digitally converting computer-aided design (CAD) designs into printing toolpaths, serpentine interconnects, and circular sensing electrodes, complex trace designs can be rapidly prototyped without photomasks. Following thermal sintering, the printed metal patterns are encapsulated with a UV-curable dielectric layer, achieving electrical insulation and electrode definition through an additive process. This workflow not only shortens the fabrication time and reduces chemical waste but also enables the fabrication of conformal MEAs that seamlessly integrate with biological surfaces for electrophysiological recording and stimulation.

To overcome the challenges associated with printing free-standing metal structures, a tension-driven conductive high-aspect-ratio metal 3D printing (CHARM3D) strategy has been developed that facilitates oxidation-stabilized deposition of molten field's metal [151]. Unlike pressure-driven direct ink writing, which disrupts the oxide layer and leads to uncontrolled droplet formation, CHARM3D draws continuous metal filaments through shear-induced tension at the nozzle–substrate interface. This fabricates smooth, self-supporting metallic architectures with high aspect ratios and tunable line widths, even on soft or irregular substrates. These capabilities open new avenues to rapidly print free-standing 3D structures for wearable electronics, fifth-generation (5G) technologies, and the Internet of Things.

Complementing these structural and fabrication advances, bioelectronics is increasingly being applied for soft, skin-integrated biochemical sensing. The solid-state epidermal biomarker (SEB) sensor exemplifies this shift, employing a multilayer screen-printed hydrogel–electrode architecture engineered for the noninvasive detection of solid-state biochemical markers directly from the stratum corneum (Fig. 12a) [152]. Its ionic-electronic hydrogel bilayer solvates and transports surface biomarkers, including hydrophobic cholesterol and hydrophilic lactate, to an enzyme-functionalized poly(3,4-ethylenedioxythiophene) (PEDOT): polystyrene sulfonate (PSS) electrode for the electrochemical readout. Combined with a flexible printed circuit board (PCB) and wireless transmission module, the SEB platform provides continuous metabolic monitoring outside clinical settings, with detection limits approaching those of mass spectrometry. Its low motion artifacts, mechanical robustness, and strong correlation with clinical gold standards illustrate the potential of soft bioelectronics for personalized and preventive healthcare.

Beyond wearable platforms, bioelectronic devices are expanding into implantable domains via soft, self-powered interface development. The tissue-adhesive piezoelectric soft sensor integrates a β-phase polyvinylidene fluoride piezoelectric film with mussel-inspired adhesive proteins to form a conformal, suture-free interface that harvests biomechanical energy from organ motion [153]. This allows real-time monitoring of cardiovascular parameters, including arterial blood pressure, heart rate, and respiration, without external power sources. Its lightweight structure, strong interfacial toughness, and high sensing fidelity during organ motion highlight the promise of mechanically compliant, energy-autonomous systems for intraoperative monitoring and long-term physiological surveillance.

As for textiles, body-coupled interactive fiber (i-fibers) development shows how bioelectronics can be woven directly into everyday materials. Through a multilayer coaxial fiber architecture containing conductive, dielectric, and electroluminescent layers, i-fibers harvest ambient electromagnetic energy through body coupling, eliminating the need for embedded chips or batteries (Fig. 12b) [154]. These fibers simultaneously function as optical emitters, sensors, and wireless transmitters, enabling applications ranging from assisted communications to smart homes to virtual reality. Furthermore, their washability, microsecond response times, and preserved softness position them as an integrated platform for next-generation wearable computing.

These advances illustrate how cutting-edge fabrication techniques, from AJP to tension-driven metal deposition, are enabling a new class of soft, adaptive, multifunctional bioelectronic systems. Whether integrated into tissues, adhered to skin, implanted within the body, or woven into fabric, these devices reveal the growing convergence of biological materials, soft engineering, and AM. Collectively, they highlight the emerging potential of bioelectronics to provide seamless, multi-modal monitoring and interaction capabilities across biomedical, wearable, and environmental applications, delineating an important frontier in bio-design and manufacturing.

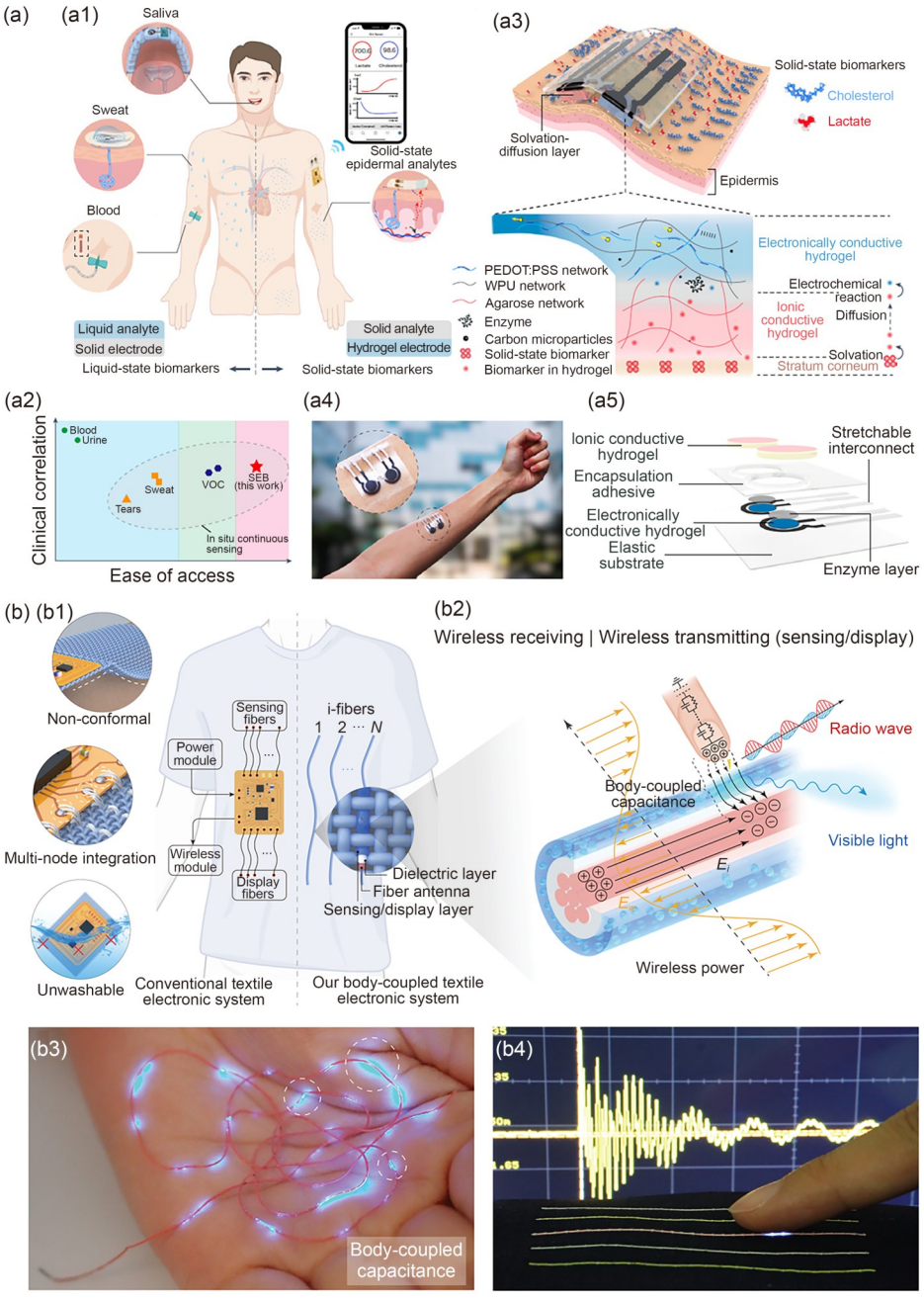

Fig. 12 Bioelectronics for epidermal sensing and interactive textiles. (a) Stretchable sensor for SEBs: (a1) a schematic illustrating the diversity of biofluids (for example, saliva, sweat, and blood) and solid-state epidermal biomarkers across different body locations, with representative sensor placements for each analyte type; (a2) comparison of biomarker accessibility and correlation with blood concentrations across liquids (blue), gaseous volatile organic compounds (green), and solid-state biomarkers (pink); (a3) illustration of an SEB sensor applied to the skin and a cross-sectional schematic of its multilayer architecture, comprising ionic conductive hydrogel (ICH), electronically conductive hydrogel (ECH), and the stratum corneum (the sensing mechanism follows a three-step sequence: solvation of solid-state biomarkers within the ICH, diffusion of the solvated species toward the ICH–ECH interface, and electrochemical reaction catalyzed within the ECH to generate detectable signals; insets depict each step in the process); (a4) photograph of the SEB sensor conformally adhered to human skin; (a5) structural schematic of the full device layout, including the SEB substrate, ECH working electrode, stretchable silver interconnections, elastic encapsulation adhesive, and the ICH solvation–diffusion layer. Reproduced from [152], under exclusive licence to Springer Nature Limited. (b) Design and operating principle of the body-coupled interactive fiber (i-fibers): (b1) conceptual comparison between conventional wireless interactive textiles relying on integrated circuit chips (left) and the chipless, body-coupled textile system enabled by the i-fibers (right); (b2) schematic of the body-coupled energy-harvesting mechanism, in which the i-fibers use the human body as a high-permittivity medium to couple ambient electromagnetic energy; (b3) photograph showing the i-fibers powered wirelessly when placed on the hand; (b4) demonstration of embroidered i-fibers generating simultaneous optical and electrical outputs upon touch, allowing chipless wireless human–textile interaction. Reproduced from [154], under exclusive license to the American Association for the Advancement of Science

5 Conclusions

Biofabrication and biomanufacturing are increasingly integrated, with the future shaped by the convergence of sustainable materials, biological systems, and precision manufacturing technologies. In this review, we focused on advances driven by research based in Singapore, highlighting how local scientific efforts are contributing to global progress in sustainable biomaterials, advanced fabrication platforms, and emerging applications. These Singapore-led studies illustrate how diverse biomass-derived feedstocks, including keratin, aquaculture byproducts, and plant polysaccharides, are expanding the library of sustainable biomaterials suitable for biomedical, food, and industrial applications. Meanwhile, biofabrication technologies such as electrospinning, 3D bioprinting, and metal AM are being actively developed and refined in Singapore to enable precise control over the structure, composition, and function of complex biological constructs.

The expanding range of application areas, including ML-assisted AM, food biomanufacturing, regenerative cell therapy, MN systems, and bioelectronics, illustrates the breadth of innovation emerging from Singapore's research landscape. These contributions highlight Singapore's strong emphasis on interdisciplinary collaboration, sustainability, and translational research. Looking ahead, continued progress in Singapore's biomanufacturing and biofabrication ecosystem will depend on advances in sustainable biomaterials, scalable bioprocessing, automated fabrication technologies, regulatory-aligned manufacturing, and data-driven optimization. As these fields become increasingly interconnected, Singapore-based research is uniquely positioned to meaningfully contribute to global developments in therapeutic, food, and industrial biotechnology. Together, these innovations reinforce Singapore's role in shaping the future of biomanufacturing and evidence how local scientific leadership can advance healthcare, material production, and societal well-being.

Author contributions WLN contributed to the conceptualization, writing, review, and editing of the manuscript. All authors contributed to the writing of the manuscript.

Declarations

Conflict of interest PB is an editorial board member of *Bio-Design and Manufacturing* (*BDM*). WLN is a young academic editor of *BDM*. They were not involved in the editorial review or the decision to publish this article. The authors declare that they have no conflict of interest.

Ethical approval This study does not contain any studies with human or animal subjects performed by any of the authors.

Use of generative AI tools During the preparation of this work, ChatGPT v5.2 was used to assist in the creation of the graphical abstract.

References

1. Ji DX, Lin YG, Guo XY et al (2024) Electrospinning of nanofibres. *Nat Rev Meth Primers* 4:1. https://doi.org/10.1038/s43586-023-00278-z
2. Ng WL, Vyas C, Huang BY et al (2025) Advanced bioprinting strategies for fabrication of biomimetic tissues and organs. *Int J Extreme Manuf* 7(6):062006. https://doi.org/10.1088/2631-7990/adeee0
3. Sing SL, Huang S, Goh GD et al (2021) Emerging metallic systems for additive manufacturing: *in-situ* alloying and multi-metal processing in laser powder bed fusion. *Prog Mater Sci* 119:100795. https://doi.org/10.1016/j.pmatsci.2021.100795
4. Ng WL, Chua CK, Shen YF (2019) Print me an organ! Why we are not there yet. *Prog Polym Sci* 97:101145. https://doi.org/10.1016/j.progpolymsci.2019.101145
5. Agarwala S, Lee JM, Ng WL et al (2018) A novel 3D bioprinted flexible and biocompatible hydrogel bioelectronic platform. *Biosens Bioelectron* 102:365–371. https://doi.org/10.1016/j.bios.2017.11.039
6. Ng WL, Sachdeva K, Conway PL et al (2025) Advanced 3D (bio)printing strategies for cultivated meat fabrication. *J Future Foods* (early access). https://doi.org/10.1016/j.jfutfo.2025.07.031
7. An J, Chua CK, Mironov V (2021) Application of machine learning in 3D bioprinting: focus on development of big data and digital twin. *Int J Bioprint* 7(1):342. https://doi.org/10.18063/ijb.v7i1.342
8. Ng WL, Chan A, Ong YS et al (2020) Deep learning for fabrication and maturation of 3D bioprinted tissues and organs. *Virtual Phys Prototyp* 15(3):340–358. https://doi.org/10.1080/17452759.2020.1771741
9. Ng WL, An J, Chua CK (2024) Process, material, and regulatory considerations for 3D printed medical devices and tissue constructs. *Engineering* 36:146–166. https://doi.org/10.1016/j.eng.2024.01.028
10. He CF, He JK, Wu CT et al (2025) 3D printing for tissue/organ regeneration in China. *Bio-Des Manuf* 8(2):169–242. https://doi.org/10.1631/bdm.2400309
11. Murphy JF, Lavelle M, Asciak L et al (2024) Biofabrication and biomanufacturing in Ireland and the UK. *Bio-Des Manuf* 7(6): 825–856. https://doi.org/10.1007/s42242-024-00316-z
12. Cao Q, Zhang Y, Deng RY et al (2023) Biomanufacturing in Japan: frontier research from 2018 to 2023. *Bio-Des Manuf* 6(6): 617–645. https://doi.org/10.1007/s42242-023-00261-3
13. Gao LJ, Liu ZX, Dikovsky D et al (2024) Innovation leading development: a glimpse into three-dimensional bioprinting in Israel. *Bio-Des Manuf* 7(3):358–382. https://doi.org/10.1007/s42242-024-00275-5
14. Su JL, Ng WL, An J et al (2024) Achieving sustainability by additive manufacturing: a state-of-the-art review and perspectives. *Virtual Phys Prototyp* 19(1):e2438899. https://doi.org/10.1080/17452759.2024.2438899
15. Reichl S (2009) Films based on human hair keratin as substrates for cell culture and tissue engineering. *Biomaterials* 30(36):6854–6866. https://doi.org/10.1016/j.biomaterials.2009.08.051
16. Wang LJ, Shang YS, Zhang J et al (2023) Recent advances in keratin for biomedical applications. *Adv Colloid Interface Sci* 321:103012. https://doi.org/10.1016/j.cis.2023.103012
17. Wang S, Taraballi F, Tan LP et al (2012) Human keratin hydrogels support fibroblast attachment and proliferation in vitro. *Cell Tissue Res* 347(3):795–802.

https://doi.org/10.1007/s00441-011-1295-2
18. Wang S, Wang ZX, Foo SEM et al (2015) Culturing fibroblasts in 3D human hair keratin hydrogels. *ACS Appl Mater Interfaces* 7(9):5187–5198. https://doi.org/10.1021/acsami.5b00854
19. Yee MZL, Lim YW, Muthualagu Natarajan L et al (2025) One-step tunable human hair keratin gradient hydrogel with antibacterial activity for tissue engineering. *Small* 21(52):e09775. https://doi.org/10.1002/smll.202509775
20. Hartrianti P, Nguyen LTH, Johanes J et al (2017) Fabrication and characterization of a novel crosslinked human keratin-alginate sponge. *J Tissue Eng Regen Med* 11(9):2590–2602. https://doi.org/10.1002/term.2159
21. Moay ZK, Nguyen LTH, Hartrianti P et al (2021) Keratin-alginate sponges support healing of partial-thickness burns. *Int J Mol Sci* 22(16):8594. https://doi.org/10.3390/ijms22168594
22. Yue K, Liu YH, Byambaa B et al (2018) Visible light crosslinkable human hair keratin hydrogels. *Bioeng Transl Med* 3(1):37–48. https://doi.org/10.1002/btm2.10077
23. Chua HM, Zhao ZT, Ng KW (2020) Cryogelation of human hair keratins. *Macromol Rapid Commun* 41(21):2000254. https://doi.org/10.1002/marc.202000254
24. Zhao ZT, Moay ZK, Lai HY et al (2021) Characterization of anisotropic human hair keratin scaffolds fabricated via directed ice templating. *Macromol Biosci* 21(2):e2000314. https://doi.org/10.1002/mabi.202000314
25. Zhao ZT, Chua HM, Goh BHR et al (2022) Anisotropic hair keratin-dopamine composite scaffolds exhibit strain-stiffening properties. *J Biomed Mater Res A* 110(1):92–104. https://doi.org/10.1002/jbm.a.37268
26. Lai HY, Setyawati MI, Ferhan AR et al (2021) Self-assembly of solubilized human hair keratins. *ACS Biomater Sci Eng* 7(1):83–89. https://doi.org/10.1021/acsbiomaterials.0c01507
27. Foo LL, Logeshwari MN, Czarny B et al (2025) Development of keratin-based fibers fabricated by interfacial polyelectrolyte complexation for suture applications. *Biomaterials* 314:122878. https://doi.org/10.1016/j.biomaterials.2024.122878
28. Schincaglia A, Pasti L, Cavazzini A et al (2024) Optimization and validation of a cheaper, safer, and more sustainable methodology for aflatoxins determination in rich-lipidic matrices (pistachio nuts) using deep eutectic solvent extraction and UHPLC-FLD analysis. *J Agric Food Chem* 72(37):20670–20678. https://doi.org/10.1021/acs.jafc.4c05094
29. Devi M, Moral R, Thakuria S et al (2023) Hydrophobic deep eutectic solvents as greener substitutes for conventional extraction media: examples and techniques. *ACS Omega* 8(11):9702–9728. https://doi.org/10.1021/acsomega.2c07684
30. Sultana R, Rashid TU, Hasan MJ et al (2025) A facile approach for enhanced keratin extraction from tannery hair waste using crude protease enzyme and optimization of hydrolysis parameters by response surface methodology. *ACS Sustainable Resour Manage* 2(3):391–401. https://doi.org/10.1021/acssusresmgt.4c00287
31. Arthur RI, Valbo-Jørgensen J, Lorenzen K et al (2023) Stocking in inland food fisheries of South and Southeast Asia: issues, risks, and rewards. *Fish Manag Ecol* 30(6):564–572. https://doi.org/10.1111/fme.12551
32. Lau CS, Hassanbhai A, Wen F et al (2019) Evaluation of decellularized tilapia skin as a tissue engineering scaffold. *J Tissue Eng Regen Med* 13(10):1779–1791. https://doi.org/10.1002/term.2928
33. Tan SH, Liu SQ, Teoh SH et al (2024) A sustainable strategy for generating highly stable human skin equivalents based on fish collagen. *Biomater Adv* 158:213780. https://doi.org/10.1016/j.bioadv.2024.213780
34. Yan PF, Zheng H, Liu P et al (2025) Ultrasound-activated piezoelectric hydrogel scaffold for synergistic immunomodulation and angiogenesis in accelerated wound healing. *Acta Biomater* 204: 216–233. https://doi.org/10.1016/j.actbio.2025.08.006
35. Wang JK, Çimenoğlu Ç, Cheam NMJ et al (2021) Sustainable aquaculture side-streams derived hybrid biocomposite for bone tissue engineering. *Mater Sci Eng C* 126:112104. https://doi.org/10.1016/j.msec.2021.112104
36. Shu KG, Huang ZQ, Pei XM et al (2023) 3D printing of high-strength photo-crosslinking flaxseed gum bioink for cartilage regeneration. *Compos Part B Eng* 263:110864. https://doi.org/10.1016/j.compositesb.2023.110864
37. Liu JH, Wang P, Gao ZH et al (2024) Review on electrospinning anode and separators for lithium ion batteries. *Renew Sustain Energy Rev* 189:113939. https://doi.org/10.1016/j.rser.2023.113939
38. Teng YJ, Song L, Shi J et al (2025) Advancing electrospinning towards the future of biomaterials in biomedical engineering. *Regen Biomater* 12:rbaf034. https://doi.org/10.1093/rb/rbaf034
39. Muthulakshmi L, Prabakaran S, Ramalingam V et al (2022) Sodium alginate nanofibers loaded *Terminalia catappa* scaffold regulates intrinsic apoptosis signaling in skin melanoma cancer. *Process Biochem* 118:92–102. https://doi.org/10.1016/j.procbio.2022.04.004
40. Rahmani F, Ziyadi H, Baghali M et al (2021) Electrospun PVP/PVA nanofiber mat as a novel potential transdermal drug-delivery system for buprenorphine: a solution needed for pain management. *Appl Sci* 11(6):2779. https://doi.org/10.3390/app11062779
41. Al-Shanqiti EM, Bawazir WA, Bakhsh EM et al (2025) Alginate and chitosan wrapped clay nanohybrid as nano-vehicles for targeted and sustained release of promethazine. *J Drug Deliv Sci Technol* 105:106548. https://doi.org/10.1016/j.jddst.2024.106548
42. Cao ZK, Zhang J, Yu YC et al (2022) Amino-modified poly (l–lactic acid) nanofibers enable pH-stimulated drug release and NIR real-time detection. *ChemNanoMat* 8(2):e202100461. https://doi.org/10.1002/cnma.202100461
43. Vigneswari S, Chai JM, Kamarudin KH et al (2020) Elucidating the surface functionality of biomimetic RGD peptides immobilized on nano-P(3HB-co-4HB) for H9c2 myoblast cell proliferation. *Front Bioeng Biotechnol* 8:567693. https://doi.org/10.3389/fbioe.2020.567693
44. Malik S, Sundarrajan S, Hussain T et al (2021) Fabrication of highly oriented cylindrical polyacrylonitrile, poly(lactide-co-glycolide), polycaprolactone and poly(vinyl acetate) nanofibers for vascular graft applications. *Polymers* 13(13):2075. https://doi.org/10.3390/polym13132075
45. Teng YJ, Zhang XH, Song L et al (2025) Construction of anticalcification small-diameter vascular grafts using decellularized extracellular matrix/poly (L-lactide-co-ε-caprolactone) and baicalin-cathepsin S inhibitor. *Acta Biomater* 197:184–201. https://doi.org/10.1016/j.actbio.2025.03.033
46. Ma YH, Wang C, Li J et al (2025) CP/HA/HGF conductive composite scaffolds with synergistic electrical stimulation for nerve regeneration. *Macromol Biosci* 25(4):e2400265. https://doi.org/10.1002/mabi.202400265
47. Vasudevan A, Majumder N, Sharma I et al (2023) Liver extracellular matrix-based nanofiber scaffolds for the culture of primary hepatocytes and drug screening. *ACS Biomater Sci Eng* 9(11): 6357–6368. https://doi.org/10.1021/acsbiomaterials.3c01216

48. Zhang S, Zhang M, Bai RB et al (2022) Electrospun coaxial nanofibers loading with perovskite and icariin to enhance the bone scaffold-mediated osteogenesis. *Mater Today Chem* 26:101246. https://doi.org/10.1016/j.mtchem.2022.101246
49. Mayandi V, Chua AWC, Dhand C et al (2020) Multifunctional antimicrobial nanofiber dressings containing ε-polylysine for the eradication of bacterial bioburden and promotion of wound healing in critically colonized wounds. *ACS Appl Mater Interfaces* 12(14): 15989–16005. https://doi.org/10.1021/acsami.9b21683
50. Ramalingam R, Dhand C, Mayandi V et al (2021) Core–shell structured antimicrobial nanofiber dressings containing herbal extract and antibiotics combination for the prevention of biofilms and promotion of cutaneous wound healing. *ACS Appl Mater Interfaces* 13(21):24356–24369. https://doi.org/10.1021/acsami.0c20642
51. Liu CL, Yang J, Bai XH et al (2021) Dual antibacterial effect of in situ electrospun curcumin composite nanofibers to sterilize drug-resistant bacteria. *Nanoscale Res Lett* 16(1):54. https://doi.org/10.1186/s11671-021-03513-2
52. Bai XH, Zhang J, Cheng GT et al (2022) Dual antibacterial polypeptide-coated PCL@ZIF-8 nanofiber reduces infection and inflammation in burn wounds. *J Mater Sci* 57(5):3678–3687. https://doi.org/10.1007/s10853-021-06832-y
53. Zhou G, Jiang LW, Qu XH et al (2025) A porous Janus nanofiber membrane with unidirectional water vapor transport for efficient dust personal protection. *Sep Purif Technol* 353:128531. https://doi.org/10.1016/j.seppur.2024.128531
54. Guo XY, Zhang QQ, Zhang CT et al (2024) Pumpless microfluidic sweat sensing yarn. *Biosens Bioelectron* 266:116713. https://doi.org/10.1016/j.bios.2024.116713
55. Reddy VS, Shiva S, Ramakrishna S (2025) Green chemistry innovation in flexible electrodes for wearable technology. *J Electron Mater* 54(11):9501–9510. https://doi.org/10.1007/s11664-025-11912-9
56. Chen N, Luo BW, Patil AC et al (2020) Nanotunnels within poly(3,4-ethylenedioxythiophene)-carbon nanotube composite for highly sensitive neural interfacing. *ACS Nano* 14(7):8059–8073. https://doi.org/10.1021/acsnano.0c00672
57. Ng WL, Yeow CHE, Huang X et al (2025) Physically crosslinked gelatin bio-inks with enhanced printability, degradation and mechanical robustness for multi-modal bioprinting. *Interdiscip Med* 3(4):e20250058. https://doi.org/10.1002/INMD.20250058
58. Li HJ, Tan YJ, Kiran R et al (2021) Submerged and non-submerged 3D bioprinting approaches for the fabrication of complex structures with the hydrogel pair GelMA and alginate/methylcellulose. *Addit Manuf* 37:101640. https://doi.org/10.1016/j.addma.2020.101640
59. Wang YX, Yue HX, Liu AD et al (2025) Dual crosslinkable bio-ink for direct and embedded 3D bioprinting at physiological temperature. *Mater Today* 85:1–16. https://doi.org/10.1016/j.mattod.2025.02.005
60. Chen SY, Shi Q, Jang T et al (2021) Engineering natural pollen grains as multifunctional 3D printing materials. *Adv Funct Mater* 31(49):2106276. https://doi.org/10.1002/adfm.202106276
61. Ates G, Bartolo P (2023) Computational fluid dynamics for the optimization of internal bioprinting parameters and mixing conditions. *Int J Bioprinting* 9(6):219. https://doi.org/10.36922/ijb.0219
62. Wang YX, Hou YH, Vyas C et al (2025) An integrated hybrid 3D bioprinting of heterogeneous and zone-specific construct resembling structural and biofunctional properties of osteochondral tissue. *Mater Futur* 4(2):025401. https://doi.org/10.1088/2752-5724/adb7f6
63. Ng WL, Shkolnikov V (2024) Optimizing cell deposition for inkjet-based bioprinting. *Int J Bioprinting* 10(2):2135. https://doi.org/10.36922/ijb.2135
64. Ng WL, Shkolnikov V (2024) Jetting-based bioprinting: process, dispense physics, and applications. *Bio-Des Manuf* 7(5):771–799. https://doi.org/10.1007/s42242-024-00285-3
65. Suntornnond R, Ng WL, Huang X et al (2022) Improving printability of hydrogel-based bio-inks for thermal inkjet bioprinting applications via saponification and heat treatment processes. *J Mater Chem B* 10(31):5989–6000. https://doi.org/10.1039/d2tb00442a
66. Ng WL, Huang X, Shkolnikov V et al (2023) Polyvinylpyrrolidone-based bioink: influence of bioink properties on printing performance and cell proliferation during inkjet-based bioprinting. *Bio-Des Manuf* 6(6):676–690. https://doi.org/10.1007/s42242-023-00245-3
67. Suntornnond R, Ng WL, Shkolnikov V et al (2024) A facile method to fabricate cell-laden hydrogel microparticles of tunable sizes using thermal inkjet bioprinting. *Droplet* 3(4):e144. https://doi.org/10.1002/dro2.144
68. Ng WL, Huang X, Shkolnikov V et al (2021) Controlling droplet impact velocity and droplet volume: key factors to achieving high cell viability in sub-nanoliter droplet-based bioprinting. *Int J Bioprint* 8(1):424. https://doi.org/10.18063/ijb.v8i1.424
69. Ng WL, Ayi TC, Liu YC et al (2021) Fabrication and characterization of 3D bioprinted triple-layered human alveolar lung models. *Int J Bioprint* 7(2):332. https://doi.org/10.18063/ijb.v7i2.332
70. Ng WL, Qi JTZ, Yeong WY et al (2018) Proof-of-concept: 3D bioprinting of pigmented human skin constructs. *Biofabrication* 10(2):025005. https://doi.org/10.1088/1758-5090/aa9e1e
71. Ng WL, Lee JM, Zhou MM et al (2020) Vat polymerization-based bioprinting: process, materials, applications and regulatory challenges. *Biofabrication* 12(2):022001. https://doi.org/10.1088/1758-5090/ab6034
72. Ng WL, Paula CTB, Serra AC et al (2026) Vat photopolymerization-based bioprinting: shaping next-generation tissues with light. *Interdiscip Med* 4(1):e70078. https://doi.org/10.1002/inmd.70078
73. Chang SY, Lee JZW, Sargur Ranganath A et al (2024) Poly(ethylene-glycol)-dimethacrylate (PEGDMA) composite for stereolithographic bioprinting. *Macromol Mater Eng* 309(11): 2400143. https://doi.org/10.1002/mame.202400143
74. Wang M, Li WL, Mille LS et al (2022) Digital light processing based bioprinting with composable gradients. *Adv Mater* 34(1): 2107038. https://doi.org/10.1002/adma.202107038
75. Kwokdinata C, Chai K, Lau K et al (2025) Bioprinted microchannel scaffolds modulate neuronal differentiation of encapsulated human spinal cord progenitor cells. *ACS Appl Bio Mater* 8(5):4337–4350. https://doi.org/10.1021/acsabm.5c00441
76. Kuah KX, Salehi M, Blackwood DJ et al (2025) Understanding the interplay of porosity on the microstructural, mechanical, and corrosion behavior of binder-jet additive-manufactured Mg-Zn-Zr alloy. *Mater Sci Eng A* 941:148649. https://doi.org/10.1016/j.msea.2025.148649
77. Salehi M, Kuah KX, Prasadh S et al (2025) Achieving biomimetic porosity and strength of bone in magnesium scaffolds through binder jet additive manufacturing. *Biomater Adv* 166:214059. https://doi.org/10.1016/j.bioadv.2024.214059

78. Salehi M, Maleksaeedi S, Bin Sapari MA et al (2019) Additive manufacturing of magnesium–zinc–zirconium (ZK) alloys via capillary-mediated binderless three-dimensional printing. *Mater Des* 169:107683. https://doi.org/10.1016/j.matdes.2019.107683
79. Kuah KX, Blackwood DJ, Ong WK et al (2022) Analysis of the corrosion performance of binder jet additive manufactured magnesium alloys for biomedical applications. *J Magnes Alloys* 10(5): 1296–1310. https://doi.org/10.1016/j.jma.2021.11.016
80. Salehi M, Kuah KX, Huang ZH et al (2023) Enhancing densification in binder jet additive manufacturing of magnesium via nanoparticles as sintering aids. *J Manuf Process* 99:705–717. https://doi.org/10.1016/j.jmapro.2023.05.096
81. Salehi M, Seet HL, Gupta M et al (2021) Rapid densification of additive manufactured magnesium alloys via microwave sintering. *Addit Manuf* 37:101655. https://doi.org/10.1016/j.addma.2020.101655
82. Salehi M, Maleksaeedi S, Nai MLS et al (2019) Towards additive manufacturing of magnesium alloys through integration of binderless 3D printing and rapid microwave sintering. *Addit Manuf* 29:100790. https://doi.org/10.1016/j.addma.2019.100790
83. Salehi M, Maleksaeedi S, Nai SML et al (2019) A paradigm shift towards compositionally zero-sum binderless 3D printing of magnesium alloys via capillary-mediated bridging. *Acta Mater* 165:294–306. https://doi.org/10.1016/j.actamat.2018.11.061
84. Salehi M, Neo DWK, Rudel V et al (2024) Digital manufacturing of personalized magnesium implants through binder jet additive manufacturing and automated post machining. *J Magnes Alloys* 12(8):3308–3324. https://doi.org/10.1016/j.jma.2024.07.027
85. Sing SL, Yeong WY, Wiria FE (2016) Selective laser melting of titanium alloy with 50 wt% tantalum: microstructure and mechanical properties. *J Alloys Compd* 660:461–470. https://doi.org/10.1016/j.jallcom.2015.11.141
86. Sing SL, Wiria FE, Yeong WY (2018) Selective laser melting of titanium alloy with 50 wt% tantalum: effect of laser process parameters on part quality. *Int J Refract Met Hard Mater* 77:120–127. https://doi.org/10.1016/j.ijrmhm.2018.08.006
87. Huang S, Sing SL, de Looze G et al (2020) Laser powder bed fusion of titanium-tantalum alloys: compositions and designs for biomedical applications. *J Mech Behav Biomed Mater* 108:103775. https://doi.org/10.1016/j.jmbbm.2020.103775
88. Sing SL, Wiria FE, Yeong WY (2018) Selective laser melting of lattice structures: a statistical approach to manufacturability and mechanical behavior. *Robot Comput Integr Manuf* 49:170–180. https://doi.org/10.1016/j.rcim.2017.06.006
89. Chua C, Sing SL, Chua CK (2023) Characterisation of in-situ alloyed titanium-tantalum lattice structures by laser powder bed fusion using finite element analysis. *Virtual Phys Prototyp* 18(1): e2138463. https://doi.org/10.1080/17452759.2022.2138463
90. Ng WL, Goh GL, Goh GD et al (2024) Progress and opportunities for machine learning in materials and processes of additive manufacturing. *Adv Mater* 36(34):2310006. https://doi.org/10.1002/adma.202310006
91. Ng WL, Tan JS (2024) Application of machine learning in 3D bioprinting of cultivated meat. *Int J AI Mater Des* 1(1):3. https://doi.org/10.36922/ijamd.2279
92. Ng WL, Tan JS (2025) Machine learning in cultivated meat: enhancing sustainability, efficiency, quality, and scalability across the production pipeline. *Food Bioprocess Technol* 18(7):5988–6009. https://doi.org/10.1007/s11947-025-03853-2
93. Huang X, Ng WL, Yeong WY (2024) Predicting the number of printed cells during inkjet-based bioprinting process based on droplet velocity profile using machine learning approaches. *J Intell Manuf* 35(5):2349–2364. https://doi.org/10.1007/s10845-023-02167-4
94. Su JL, Chen LQ, Van Petegem S et al (2025) Additive manufacturing metallurgy guided machine learning design of versatile alloys. *Mater Today* 88:240–250. https://doi.org/10.1016/j.mattod.2025.06.031
95. Liu YT, Su JL, Li YH et al (2025) In-situ alloying modulation in additive manufacturing of titanium-tantalum alloy: from melt pool modelling to process development. *Mater Sci Eng R Rep* 166:101082. https://doi.org/10.1016/j.mser.2025.101082
96. Liu YT, Chua C, Soh V et al (2025) Revealing the underlying mechanism in controlling Young's modulus of additively manufactured Ti-6Al-4V using fuzzified machine learning. *Virtual Phys Prototyp* 20(1):e2443103. https://doi.org/10.1080/17452759.2024.2443103
97. Williams RJ, Sing SL (2025) Spatiotemporal analysis of powder bed fusion melt pool monitoring videos using deep learning. *J Intell Manuf* 36(4):2409–2422. https://doi.org/10.1007/s10845-024-02355-w
98. Zhang JY, Farbiz F, Jafary-Zadeh M et al (2025) From detection to forecasting: utilizing time-series foundation models to anticipate defects in metal additive manufacturing. *J Manuf Process* 150:1040–1052. https://doi.org/10.1016/j.jmapro.2025.06.056
99. Su LS, Jing LZ, Zeng XJ et al (2023) 3D-printed prolamin scaffolds for cell-based meat culture. *Adv Mater* 35(2):2207397. https://doi.org/10.1002/adma.202207397
100. Mi JQ, Guo ZN, Qian HQ et al (2025) Sustainable food-grade serum-reducing biomaterial: plant protein hydrolysates for scalable cultivated meat manufacturing. *Chem Eng J* 519:164496. https://doi.org/10.1016/j.cej.2025.164496
101. Murugan P, Yap WS, Ezhilarasu H et al (2024) Decellularised plant scaffolds facilitate porcine skeletal muscle tissue engineering for cultivated meat biomanufacturing. *npj Sci Food* 8(1):25. https://doi.org/10.1038/s41538-024-00262-1
102. Tay JU, Zhou CY, Lee HW et al (2023) 3D printing of salmon fillet mimic: imparting printability via high-pressure homogenization and post-printing texturization via transglutaminase. *Food Hydrocoll* 140:108564. https://doi.org/10.1016/j.foodhyd.2023.108564
103. Tan JS, Ng WL (2025) 3D printing of salmon sashimi analogues using fish-derived food inks: printability, texture, and nutritional evaluation. *Food Bioprocess Technol* 18(10):8539–8553. https://doi.org/10.1007/s11947-025-03943-1
104. Zhou HZ, Loo LSW, Ong FYT et al (2025) Cost-effective production of meaty aroma from porcine cells for hybrid cultivated meat. *Food Chem* 473:142946. https://doi.org/10.1016/j.foodchem.2025.142946
105. Pant A, Lee AY, Karyappa R et al (2021) 3D food printing of fresh vegetables using food hydrocolloids for dysphagic patients. *Food Hydrocoll* 114:106546. https://doi.org/10.1016/j.foodhyd.2020.106546
106. Pant A, Ni Leam PX, Chua CK et al (2023) Valorisation of vegetable food waste utilising three-dimensional food printing. *Virtual Phys Prototyp* 18(1):e2146593. https://doi.org/10.1080/17452759.2022.2146593
107. Pakseresht A, Ahmadi Kaliji S, Canavari M (2022) Review of factors affecting consumer acceptance of cultured meat. *Appetite* 170:105829. https://doi.org/10.1016/j.appet.2021.105829

108. Scharfmann R, Pechberty S, Hazhouz Y et al (2014) Development of a conditionally immortalized human pancreatic β cell line. *J Clin Invest* 124(5):2087–2098. https://doi.org/10.1172/JCI72674
109. Loo LSW, Lau HH, Jasmen JB et al (2018) An arduous journey from human pluripotent stem cells to functional pancreatic β cells. *Diabetes Obes Metab* 20(1):3–13. https://doi.org/10.1111/dom.12996
110. Lim LY, Ching C, Kong DW et al (2022) Generating pancreatic beta-like cells from human pluripotent stem cells. *Meth Cell Biol* 170:127–146. https://doi.org/10.1016/bs.mcb.2022.02.011
111. Teo AKK, Windmueller R, Johansson BB et al (2013) Derivation of human induced pluripotent stem cells from patients with maturity onset diabetes of the young. *J Biol Chem* 288(8):5353–5356. https://doi.org/10.1074/jbc.C112.428979
112. Teo AKK, Lau HH, Valdez IA et al (2016) Early developmental perturbations in a human stem cell model of MODY5/HNF1B pancreatic hypoplasia. *Stem Cell Rep* 6(3):357–367. https://doi.org/10.1016/j.stemcr.2016.01.007
113. Ng NHJ, Jasmen JB, Lim CS et al (2019) HNF4A haploinsufficiency in MODY1 abrogates liver and pancreas differentiation from patient-derived induced pluripotent stem cells. *iScience* 16:192–205. https://doi.org/10.1016/j.isci.2019.05.032
114. Low BSJ, Lim CS, Ding SSL et al (2021) Decreased GLUT2 and glucose uptake contribute to insulin secretion defects in MODY3/HNF1A hiPSC-derived mutant β cells. *Nat Commun* 12(1):3133. https://doi.org/10.1038/s41467-021-22843-4
115. Amirruddin NS, Tan WX, Tan YS et al (2021) Progressive endoplasmic reticulum stress over time due to human insulin gene mutation contributes to pancreatic beta cell dysfunction. *Diabetologia* 64(11):2534–2549. https://doi.org/10.1007/s00125-021-05530-3
116. Chan JW, Neo CWY, Ghosh S et al (2023) HNF1A binds and regulates the expression of SLC51B to facilitate the uptake of estrone sulfate in human renal proximal tubule epithelial cells. *Cell Death Dis* 14(5):302. https://doi.org/10.1038/s41419-023-05827-8
117. Lau HH, Krentz NAJ, Abaitua F et al (2023) PAX4 loss of function increases diabetes risk by altering human pancreatic endocrine cell development. *Nat Commun* 14(1):6119. https://doi.org/10.1038/s41467-023-41860-z
118. Nguyen L, Chan SY, Teo AKK (2018) Metformin from mother to unborn child—are there unwarranted effects? *EBioMedicine* 35:394–404. https://doi.org/10.1016/j.ebiom.2018.08.047
119. Nguyen L, Lim LY, Ding SSL et al (2021) Metformin perturbs pancreatic differentiation from human embryonic stem cells. *Diabetes* 70(8):1689–1702. https://doi.org/10.2337/db20-0722
120. Li JH, Inoue R, Togashi Y et al (2022) Imeglimin ameliorates β-cell apoptosis by modulating the endoplasmic reticulum homeostasis pathway. *Diabetes* 71(3):424–439. https://doi.org/10.2337/db21-0123
121. Ng NHJ, Ghosh S, Bok CM et al (2024) HNF4A and HNF1A exhibit tissue specific target gene regulation in pancreatic beta cells and hepatocytes. *Nat Commun* 15(1):4288. https://doi.org/10.1038/s41467-024-48647-w
122. Tan LS, Chen JT, Lim LY et al (2022) Manufacturing clinical-grade human induced pluripotent stem cell-derived beta cells for diabetes treatment. *Cell Prolif* 55(8):e13232. https://doi.org/10.1111/cpr.13232
123. Lim LY, Ding SSL, Muthukumaran P et al (2023) Tissue engineering of decellularized pancreas scaffolds for regenerative medicine in diabetes. *Acta Biomater* 157:49–66. https://doi.org/10.1016/j.actbio.2022.11.032
124. Soetedjo AAP, Lee JM, Lau HH et al (2021) Tissue engineering and 3D printing of bioartificial pancreas for regenerative medicine in diabetes. *Trends Endocrinol Metab* 32(8):609–622. https://doi.org/10.1016/j.tem.2021.05.007
125. Zhang T, Yam GH, Riau AK et al (2013) The effect of amniotic membrane de-epithelialization method on its biological properties and ability to promote limbal epithelial cell culture. *Invest Ophthalmol Vis Sci* 54(4):3072–3081. https://doi.org/10.1167/iovs.12-10805
126. Bandeira F, Yam GH, Fuest M et al (2019) Urea-de-epithelialized human amniotic membrane for ocular surface reconstruction. *Stem Cells Transl Med* 8(7):620–626. https://doi.org/10.1002/sctm.18-0201
127. Li Z, Goh TW, Yam GH et al (2019) A sintered graphene/titania material as a synthetic keratoprosthesis skirt for end-stage corneal disorders. *Acta Biomater* 94:585–596. https://doi.org/10.1016/j.actbio.2019.05.053
128. Riau AK, Look Z, Yam GHF et al (2024) Impact of keratocyte differentiation on corneal opacity resolution and visual function recovery in male rats. *Nat Commun* 15(1):4959. https://doi.org/10.1038/s41467-024-49008-3
129. Ma Q, Riau AK, Young RD et al (2025) Ultrastructural aspects of corneal functional recovery in rats following intrastromal keratocyte injection. *Invest Ophthalmol Vis Sci* 66(2):45. https://doi.org/10.1167/iovs.66.2.45
130. Riau AK, Angunawela RI, Chaurasia SS et al (2013) Reversible femtosecond laser-assisted myopia correction: a non-human primate study of lenticule re-implantation after refractive lenticule extraction. *PLoS ONE* 8(6):e67058. https://doi.org/10.1371/journal.pone.0067058
131. Liu YC, Teo EPW, Ang HP et al (2018) Biological corneal inlay for presbyopia derived from small incision lenticule extraction (SMILE). *Sci Rep* 8(1):1831. https://doi.org/10.1038/s41598-018-20267-7
132. Nubile M, Salgari N, Mehta JS et al (2021) Epithelial and stromal remodelling following femtosecond laser-assisted stromal lenticule addition keratoplasty (SLAK) for keratoconus. *Sci Rep* 11(1):2293. https://doi.org/10.1038/s41598-021-81626-5
133. Riau AK, Boey KPY, Yusoff NZBM et al (2022) Experiment-based validation of corneal lenticule banking in a health authority-licensed facility. *Tissue Eng Part A* 28(1–2):69–83. https://doi.org/10.1089/ten.TEA.2021.0042
134. Soo JYW, Tan G, Han E et al (2025) Impact of transportation on the suitability of cryopreserved corneal lenticule for implantation. *ACS Appl Bio Mater* 8(3):2065–2077. https://doi.org/10.1021/acsabm.4c01632
135. Thirunavukarasu AJ, Han E, Nedumaran AM et al (2023) Electron beam-irradiated donor cornea for on-demand lenticule implantation to treat corneal diseases and refractive error. *Acta Biomater* 169:334–347. https://doi.org/10.1016/j.actbio.2023.07.053
136. Mastropasqua L, Nubile M, Acerra G et al (2022) Bioengineered human stromal lenticule for recombinant human nerve growth factor release: a potential biocompatible ocular drug delivery system. *Front Bioeng Biotechnol* 10:887414. https://doi.org/10.3389/fbioe.2022.887414
137. Ong HS, Peh G, Neo DJH et al (2020) A novel approach of harvesting viable single cells from donor corneal endothelium for cell-injection therapy. *Cells* 9(6):1428. https://doi.org/10.3390/cells9061428

138. Peh GSL, Ang HP, Lwin CN et al (2017) Regulatory compliant tissue-engineered human corneal endothelial grafts restore corneal function of rabbits with bullous keratopathy. *Sci Rep* 7(1): 14149. https://doi.org/10.1038/s41598-017-14723-z
139. Peh GSL, Ong HS, Adnan K et al (2019) Functional evaluation of two corneal endothelial cell-based therapies: tissue-engineered construct and cell injection. *Sci Rep* 9(1):6087. https://doi.org/10.1038/s41598-019-42493-3
140. Loh JM, Lim YJL, Tay JT et al (2024) Design and fabrication of customizable microneedles enabled by 3D printing for biomedical applications. *Bioact Mater* 32:222–241. https://doi.org/10.1016/j.bioactmat.2023.09.022
141. Wang M, Han YY, Yu XJ et al (2020) Upconversion nanoparticle powered microneedle patches for transdermal delivery of siRNA. *Adv Healthc Mater* 9(2):1900635. https://doi.org/10.1002/adhm.201900635
142. Chun YY, Tan WWR, Vos MIG et al (2022) Scar prevention through topical delivery of gelatin-tyramine-siSPARC nanoplex loaded in dissolvable hyaluronic acid microneedle patch across skin barrier. *Biomater Sci* 10(14):3963–3971. https://doi.org/10.1039/d2bm00572g
143. Lim DZJ, Chun YY, Tan FNSY et al (2024) Small interfering RNA microneedle patches versus silicone sheets in reducing postoperative scars: a randomized single-blinded intraindividually controlled clinical trial. *Br J Dermatol* 192(1):19–26. https://doi.org/10.1093/bjd/ljae347
144. Le ZC, Shou YF, Li RR et al (2024) Sponge-like microneedles spatially sequester chemokines and deplete monocytes to alleviate inflammatory skin disorders. *Adv Funct Mater* 34(41):2402539. https://doi.org/10.1002/adfm.202402539
145. Zan P, Than A, Leow MKS et al (2024) Dry powder microneedle-enabled transdermal anti-inflammatory therapy for obesity, diabetes, hyperlipidemia, and fatty liver. *Chem Eng J* 484:149395. https://doi.org/10.1016/j.cej.2024.149395
146. Chang H, Chew SWT, Zheng MJ et al (2021) Cryomicroneedles for transdermal cell delivery. *Nat Biomed Eng* 5(9):1008–1018. https://doi.org/10.1038/s41551-021-00720-1
147. Cui MY, Zheng MJ, Wiraja C et al (2021) Ocular delivery of predatory bacteria with cryomicroneedles against eye infection. *Adv Sci* 8(21):2102327. https://doi.org/10.1002/advs.202102327
148. Zheng MJ, Wang ZF, Chang H et al (2020) Osmosis-powered hydrogel microneedles for microliters of skin interstitial fluid extraction within minutes. *Adv Healthc Mater* 9(10):1901683. https://doi.org/10.1002/adhm.201901683
149. Liang K, Leong C, Loh JM et al (2022) A 3D-printed transepidermal microprojection array for human skin microbiome sampling. *Proc Natl Acad Sci USA* 119(30):e2203556119. https://doi.org/10.1073/pnas.2203556119
150. Cheah E, Gao XC, Jaw WQ et al (2026) Customizable fabrication of 2D and conformal multielectrode arrays for 3D printed organotypic bioelectronic interfaces. *Adv Healthc Mater* 15(8): e02757. https://doi.org/10.1002/adhm.202502757
151. Ling SH, Tian X, Zeng QH et al (2024) Tension-driven three-dimensional printing of free-standing Field's metal structures. *Nat Electron* 7(8):671–683. https://doi.org/10.1038/s41928-024-01207-y
152. Arwani RT, Tan SCL, Sundarapandi A et al (2024) Stretchable ionic-electronic bilayer hydrogel electronics enable in situ detection of solid-state epidermal biomarkers. *Nat Mater* 23(8):1115–1122. https://doi.org/10.1038/s41563-024-01918-9
153. Wang C, Hu YR, Liu Y et al (2023) Tissue-adhesive piezoelectric soft sensor for in vivo blood pressure monitoring during surgical operation. *Adv Funct Mater* 33(38):2303696. https://doi.org/10.1002/adfm.202303696
154. Yang WF, Lin SM, Gong W et al (2024) Single body-coupled fiber enables chipless textile electronics. *Science* 384(6691):74–81. https://doi.org/10.1126/science.adk3755